Faculty Mechanical, Maritime and Materials Engineering

MSc Offshore and Dredging Engineering

Master Thesis

A Finite Element Analysis Investigation of Fatigue and Corrosion of Floating Offshore Wind Turbine Mooring Lines

Author:

Theresa Marie Beer

5569435

Supervisor:

Dr. Andrea Coraddu

Dr. Olena Karpenko

16.10.2023

1 Abstract

With the rising demand for renewable energy, floating offshore wind turbines have gained importance, particularly in regions where deep waters prevent the use of traditional monopile structures. These floating turbines rely on mooring lines for stability against environmental conditions, particularly when facing strong winds and high waves.

Ensuring a satisfactory lifetime and health of mooring lines is critical. Moreover, degradation can compromise the turbine's functionality or even lead to catastrophic failures. While direct monitoring is ideal, it is often hampered by high costs and extensive maintenance.

This Master's thesis introduces a novel method to assess mooring line degradation. The proposed approach simulates the impact of environmental conditions on the mooring lines, considering various forces and weather scenarios.

The research presents modeling of fatigue and corrosion effects along the mooring line. A unique corrosion model calculates variations based on seawater's oxygen and temperature profiles.

Concurrently, mooring line stresses are deduced from real-world environmental conditions. Integrating these, a finite element model is constructed to analyze different load scenarios and the onset of corrosion on line degradation. The model considers the joint impact of corrosion and fatigue on mooring lines, including the influence of hydro static pressure and out-of-plane bending. Validation of this methodology draws upon existing research and experimental results on mooring lines.

2 Preface

The following Master's thesis was carried out in connection with the Offshore Engineering and Dredging Master's program at TU Delft. It was carried out as a final requirement to complete the Master's in cooperation with the department 3ME.

Before presenting the thesis, I would like to sincerely thank the people who have supported me throughout this process.

I would like to thank my supervisors, Dr Andrea Corradu and Dr Olena Karpenko. who not only supervised me but were always available for advice and assistance. Thank you for the comprehensive supervision and your guidance at every stage of my thesis process. Thank you for always having an open time slot for me and my questions.

Special appreciation goes to my mother, Sandra, and my stepfather, Matthias, who took me in during my thesis and always provided words of encouragement and motivation throughout my studies. I want to especially thank my mother for her constant support, inspiration, and much more. Without you, my studies would not have been possible.

I would also like to thank Jannis Molter, Jan-Philipp Grünther, Janina Klein, and Anneke Neber for proofreading my thesis. Thank you for your support and grammatical awareness.

Finally, I would like to thank all the people and friends who accompanied me during my studies at TU Delft, who made the ups and downs of a Master's degree so bearable and fun. I would like to thank the staff of the Master of Offshore and Dredging Engineering for this tremendous academic experience and the constant help throughout the program.

Affidavit

I, Theresa Beer, born on 11.08.1998 in Dresden, declare this thesis was written independently. No other aids or sources were used, than those listed. Passages which are taken literally or analogously from sources have been clearly marked as such. The work has not been submitted in the same or similar form to any other examination office. I am aware that a false declaration will have legal consequences.

Signed: T.M.B

Date: 16.10.2023

Contents

List of Figures

List of Tables

Nomenclature

ρ Density of the liquid

d Water depth

d_0 reference height

L_i Amplitude of load

m S-N curve slope

n_i Cycles of Load

N_{raf} reference cycle number

P Hydro static pressure

$v_{c,\,\text{tide}}(0)$ current velocity at the reference depth

$v_{c,wind}(0)$ wind speed measured at the reference height

z depth

d Diameter

Acronyms

3 Introduction

Due to changes in energy demand in recent years, more wind energy is needed to facilitate the transition from fossil fuels to renewable energy. Therefore, more and more wind turbines are being built, especially offshore, where space is available and wind can flow freely without obstructions. By the end of 2027, the total installed offshore wind capacity in Europe is expected to reach 37 gigawatts (GW) [2]. As most of these wind turbines are installed using bottom-founded monopiles, less space is available in the shallower parts of the oceans.

This has led to the development of floating offshore wind turbines (FOWT), which allow wind energy to be generated in deeper waters. Unlike conventional offshore wind turbines, these turbines are not installed on a monopile on the seabed but on floating pontoons held in place by mooring lines. Especially for countries without shelf seas need turbines, which do not have to be installed in the ground, this is a good alternative to meet the demand for renewable energy [3].

The first floating offshore wind farm was installed in 2017, and since then, the installed capacity of floating offshore wind in Europe has reached 73.33 megawatts (MW) [4]. But with innovation, often new problems arise. As reported by *Fontaine et al.* [5], half of the turbine failures were caused by mooring line failure, of which half were caused by **corrosion** and **fatigue**. These numbers reflect the situation in the oil and gas industry, which has been using mooring lines to secure floating production units since 1977 [6].

As this problem is not new to the offshore industry, but has been an obstacle for years, it has resulted in lost investment for decades [5]. To solve this issue, studies have been carried out, and further mooring line models have been developed to identify the roots and possible solutions.

At the beginning of the thesis procedure, a literature study was carried out to analyze the literature and examine the current data. It was found that although some research considers fatigue and corrosion, these influences are often implemented as a constant influence along the mooring line or over its lifetime. An implementation like this can be unspecific since loads vary along the mooring line, and corrosion varies over the water column. Further, most of the studies are carried out based on floating production storage and offloading units (FPSOs), which are secured with a higher number of mooring lines and with different mooring systems.

Therefore, the following Master's thesis will be based on the research question "How can fatigue and corrosion be modeled to identify weak points along the mooring lines of floating offshore wind turbines?" established in the literature review.

In order to answer this question, the following Master's thesis will be carried out and divided into several chapters. Chapter 4 summarises the theoretical foundations established in the literature review. The case study on which the project was built is described in detail in chapter 5. Based on this, the methodological structure is explained in chapter 6. The results are presented in chapter 7, and the discussion of these is executed in chapter 8. Finally, in chapter 9, a conclusion is drawn about the experiments and the research questions.

4 Literature review summary

Prior to this work, a literature review was carried out to identify current research on mooring line degradation. In this literature review, special consideration was given to the effects of fatigue and corrosion. Both can cause a reduction in the lifetime of mooring lines. In the following paragraphs, a summary of the results is given. The entire literature review can be found in Appendix A.

Corrosion is found to reduce the lifetime through the weakening of the mooring line material. Mooring lines immersed in seawater were found to develop corrosion based on the influences of oxygen, temperature, bacteria, salinity, and water on steel [7]. In the development process of corrosion in steel, first, corrosion pits are created. These develop horizontally towards uniform corrosion, leading to an overall reduction of diameter [8]. This reduction can cause a shorter lifetime of the mooring line as the material strength decreases.

The research that has been carried out regarding mooring line corrosion is often limited as it requires time and funding to be executed. Further, mooring lines are often only investigated in specific points as the analysis of the whole length would require a high amount of resources. One often neglected impact is how corrosion develops along the mooring line. As described by *Orlikowsko et al.* [9], the factors influencing corrosion vary over water depth, which could lead to a variation of corrosion alone the mooring line dependent on the water depth.

Fatigue is often caused by cyclic loads leading to crack initiation and development. These cracks can form at either corrosion pits or critical high-stress sections of the mooring line and then develop through cyclic loading[10]. They can decrease the lifetime of a mooring line substantially. If the cracks come to a critical depth, the mooring line can rip, leading to dangerous failure events [11].

A combination of fatigue and corrosion can reduce the lifetime and has to be accounted for. To determine the fatigue life of a material, S-N curves are utilized [12]. S-N curves describe how many cycles in a stress range a material can endure until fatigue occurs. As presented by *Lone et al.* [13], new S-N curves have been developed to include corrosion in the fatigue lifetime assessment. One problem in these predictions is that corrosion is implemented conservatively as a steady factor [14]. This could lead to underestimating the real corrosion value depending on the variation within the water depth and immersion time.

Additionally, no research has been executed regarding these two mechanisms causing specific weak points along the mooring line. This leads to the question of whether the change of corrosion and fatigue along the mooring line has an impact and can lead to a higher deterioration in specific areas. Even though some papers state that particular regions are more prone to failure than other regions along the mooring line, none has examined corrosion and fatigue influences in these regions.

Based on these findings, the following main research question was identified:

How can fatigue and corrosion be modeled to identify weak points along the mooring lines of floating offshore wind turbines?

The following sub-questions will be addressed in more detail:

- How can fatigue be accurately modeled along the mooring line?
- How can corrosion be accurately modeled along the mooring line?
- How do fatigue and corrosion interact?
- How can the weak points be improved?

5 Case study

The following chapter presents the case study on which the Master's thesis was conducted. As part of the research methodology is based on this study and relies on the previous presentation, it is presented first, followed by another chapter regarding the method itself.

As a basis for the case study, a sample FOWT was selected on which the procedure described in chapter 6 was carried out. In order to identify this FOWT, several requirements had to be met. Firstly, open-source details of the site, turbine, substructure, and mooring configuration were required. Further, environmental data, mooring chain material, and additional information such as seabed conditions were necessary for later implementation in the finite element model (FEM). In addition, the designed FOWT had to be developed recently to produce a result based on state-of-the-art FOWT and thus be a contribution to current and future research.

Based on these requirements, three open-source FOWT studies were identified as a possible basis for the project. The first was the Hywind project, well known in the research community as the first FOWT project to be installed in Scotland [15].
Secondly, the Lifes 50+ project developed a FOWT based on a 10MW turbine with two substructure configurations at three different sites [16].
Finally, the FOWT published within the COREWIND project, is based on a 15 MW turbine operating at three sites with two different substructure configurations [1]. The specifications for all presented projects can be found in Table 1.

Project	**Hywind[15]**	**Lifes50+[16]**	**COREWIND[1]**
Year of publication	2017	2019	2023
Turbine	OC3	OO-Star Wind Nautilus 10	IEA Wind 15
Capacity	5MW	10MW	15MW
Location	Scotland	France Scotland USA	Spain Scotland USA
Substructure	Spar	Semi-submersible	Spar Semi-submersible
Mooring system design	Catenary Mooring lines	Different Configurations	Catenary Mooring system
Open-source	Yes	Yes	Yes
OpenFast model available	Yes	Yes	Yes

Table 1: Comparison of FOWT open-source projects.

Table 1 shows that COREWIND is the most recent project and provides open-source data and specifications. It was, therefore, decided to base the case study on the COREWIND project. As there are two substructure types, each combined with three different locations and mooring settings, a further decision had to be made to narrow down the final setup for the case study. After a short introduction of the COREWIND project itself, the decision process is presented in the following paragraphs.

The COREWIND project is an open-source project funded by the European Union to develop floating wind projects further. In this project, an IEA 15 MW wind turbine was placed on two different floating sub-platforms in three possible areas. This project provides the latest details of possible offshore floating wind turbines so it can be used as a research database. The project's scope had to be narrowed to one substructure and the site. The first decision was the location of the site. The sites are in Scotland, North West Africa, and California and are compared in Table 2 below.

Site	**West of Barra**	**Gran Canaria**	**Morro Bay**
Coordinates	N7°56′52.84″	N27°45′0.00″	N35°5′0.00″
	W56°53′9.60″	W15°19′48.00″	W121°30′0.00″
Area	Scotland	Canary Islands (Spain)	California (Usa)
Water Depth [m]	100	200	870
Seabed type	Rock	Continuous layer of sand	Medium dense sands

Table 2: Comparison of the three different locations of the COREWIND project.

Gran Canaria was chosen as the preferred location due to its developed Open Fast model and the water depth. As described in the previous literature review, if the water is too shallow, there can be effects on the mooring line that increase the loads [17]. This can be difficult to model, so a relatively deep site should be chosen. However, the depth should be manageable as the modeling of the FEM gets more extensive with a longer chain. Therefore, the intermediate depth of the Gran Canaria site was chosen. The OpenFast model, also available for this site, includes the semi-submersible substructure.

5.1 COREWIND location

Gran Canaria is an island in the Canary Islands archipelago, located west of the African continent. The exact location of the COREWIND project is at W15°19′48.00″ N27°45′0.00″ as mentioned above. The location of the proposed to Gran Canaria is shown in Figure 1. This exact location has been used to collect environmental data throughout the project. The environmental data is presented in the following sections.

Figure 1: Location of the basis FOWT near Gran Canaria [1].

5.2 Environmental Data

In order to determine the loads on the turbine, substructure, and mooring lines of the FOWT in the later thesis, the environmental loads must be analyzed. In the following subchapters, the environmental data extracted from the COREWIND project are presented in relation to wind, waves, and currents. Although they usually interfere with and influence each other, these variables are presented separately in combined scatter plots. Temperature and oxygen at different depths are extracted from the World Ocean Atlas (WOA) at the Gran Canaria site and will be presented in the following methodology in regard to the later corrosion study.

5.2.1 Wind data at COREWIND location

The wind frequency and direction in the location southeast of Gran Canaria are presented in Table 3 and Figure 2.

Wind speed range [m/s]		Frequency (%)
0.0	1.5	2.30%
1.5	3.0	7.70%
3.0	4.5	13.15%
4.5	6.0	18.90%
6.0	7.5	21.35%
7.5	9.0	18.15%
9.0	10.5	10.80%
10.5	12.0	4.80%
12.0	13.5	1.80%
13.5	15.0	0.70%
15.0	16.5	0.25%
16.5	18.0	0.05%
18.0	19.5	0.05%

Table 3: Wind speed ranges are plotted in relation to occurring frequency. In a row, the first value is the lower boundary, and the second value is the upper boundary of a wind range [1].

As seen in Table 3, the most prevalent wind range is 6 - 7.5 m/s with a share of 21.35 % . In Figure 2, the wind is divided according to the incoming flow direction. The most common direction is north-north-east, with a probability of about 46%.

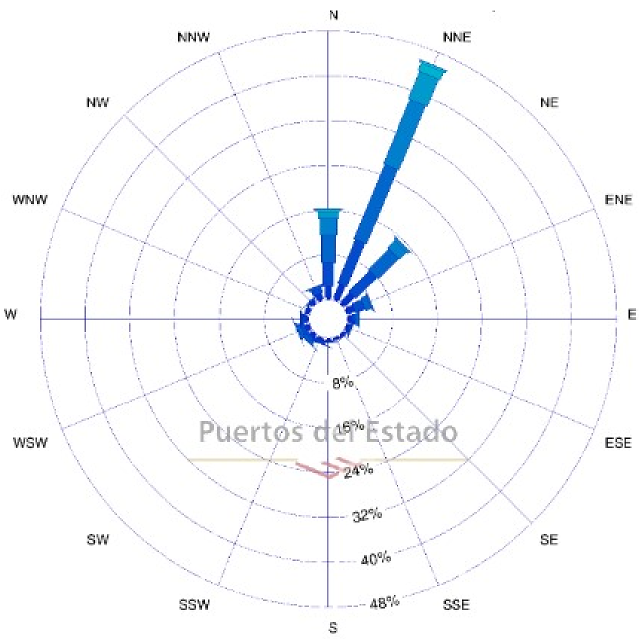

Figure 2: The wind rose for the wind occurring at the Gran Canaria location. The wind inflow direction is plotted regarding the probability of occurrence [1].

5.2.2 Wave data at COREWIND location

Concerning wave properties and occurrence, additional detailed data has been provided by the COREWIND project. The figures extracted for the wave data at the Gran Canaria site are presented below. In Table 4, the wave height is plotted in combination with the peak period in relation to their combined occurrence, which gives an estimate of the wave spectrum.

%		Significant Wave Height (m)					
		0-1	1-2	2-3	3-4	4-5	Total
Peak Period (s)	1-2	0.037	0.001	0	0	0	0.038
	2-3	0.771	0.3	0	0	0	1.071
	3-4	2.603	1.845	0	0	0	4.448
	4-5	4.524	5.132	0.003	0	0	9.659
	5-6	5.392	10.973	0.049	0	0	16.414
	6-7	4.907	14.608	0.465	0	0	19.980
	7-8	4.211	9.569	2.593	0.012	0	16.385
	8-9	3.504	5.006	2.552	0.11	0	11.172
	9-10	2.836	3.119	1.087	0.147	0.001	7.190
	10-11	2.252	1.865	0.522	0.073	0.003	4.715
	11-12	1.766	1.250	0.275	0.028	0	3.319
	12-13	1.244	0.823	0.161	0.005	0	2.233
	13-14	0.827	0.542	0.12	0.001	0	1.490
	14-15	0.512	0.326	0.085	0.002	0	0.925
	15-16	0.27	0.21	0.052	0.003	0	0.535
	16-17	0.129	0.119	0.034	0.001	0	0.283
	17-18	0.04	0.058	0.005	0	0	0.103
	18-19	0.01	0.018	0	0	0	0.028
	19-20	0.001	0.006	0.001	0	0	0.008
	20-21	0	0.002	0	0	0	0.002
	21-22	0	0.001	0	0	0	0.001
	Total	35.84	55.77	8.004	0.382	0.004	100.000

Table 4: Scatter diagram for wave height and peak period. Wave height and peak period are plotted regarding their combined probability of occurrence [1].

In addition, the wave direction has been plotted in relation to the significant wave height. As shown in Table 5, the most prominent combination is a wave propagation from the north with a height of 1 to 1.5 meters.

The dominant wave direction is also shown in Figure 3, as the two most dominant wave directions are from north and north-north-east with a probability of 52% and 40 %, respectively.

		Wave direction (°)							
		0	45	90	135	180	225	270	315
Hs (m)	0.0-0.5	1.154	0.439	0.059	0.017	0.004	0.000	0.171	0.322
	0.5-1.0	10.887	7.317	0.591	0.094	0.033	0.262	0.631	0.912
	1.0-1.5	17.103	14.722	0.892	0.155	0.042	0.569	0.431	0.661
	1.5-2.0	12.711	11.966	0.556	0.066	0.019	0.362	0.141	0.094
	2.0-2.5	5.260	5.626	0.105	0.012	0.017	0.122	0.012	0.011
	2.5-3.0	1.809	2.180	0.018	0.000	0.001	0.050	0.015	0.010
	3.0-3.5	0.387	0.530	0.000	0.000	0.004	0.056	0.001	0.000
	3.5-4.0	0.100	0.163	0.000	0.000	0.004	0.016	0.000	0.000
	4.0-4.5	0.001	0.060	0.000	0.000	0.000	0.000	0.000	0.000
	4.5-5.0	0.000	0.024	0.000	0.000	0.000	0.000	0.000	0.000
	5.0-10	0.000	0.004	0.000	0.000	0.000	0.000	0.000	0.000

Table 5: Wave direction and Wave height plotted in regard to their combined probability of occurence [1].

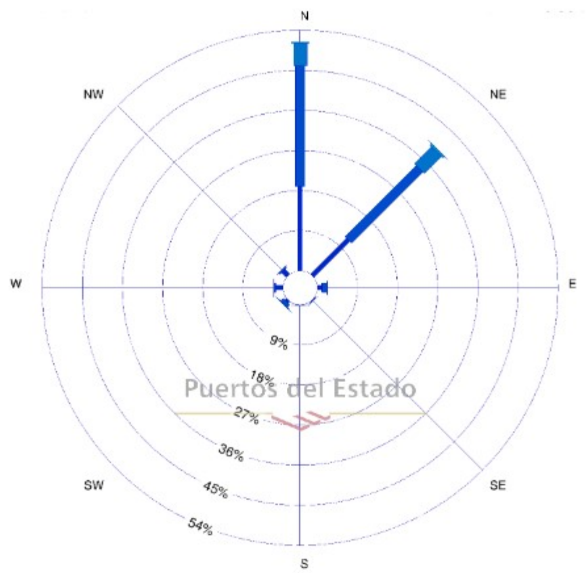

Figure 3: Wave direction distribution near Gran Canaria. Wave rose for the wind at the Gran Canaria location, wave direction is plotted in regard to the probability of occurrence [1].

Significant Wave Height [m]	WIND SPEED (1-hour at 10 m)										
	0.00 - 2.00	2.00 - 4.00	4.00 - 6.00	6.00 - 8.00	8.00 - 10.00	10.00 - 12.00	12.00 - 14.00	14.00 - 16.00	16.00 - 18.00	18.00 - 20.00	>20.00
0.00 - 1.00	2.083	8.396	12.354	8.754	4.174	1.685	0.588	0.144	0.044	0.010	0.001
1.00 - 2.00	3.012	12.063	18.533	12.298	5.582	2.195	0.777	0.248	0.062	0.010	0.006
2.00 - 3.00	0.384	1.387	2.041	1.568	0.785	0.295	0.126	0.055	0.012	0.003	0.002
3.00 - 4.00	0.014	0.060	0.109	0.076	0.034	0.009	0.007	0.003			
4.00 - 5.00			0.005	0.003							
5.00 - 6.00											
6.00 - 7.00											
> 7.00											

Table 9.4-1 – Wind – Wave scatter diagram

Figure 4: Scatter diagram of the wind speed and significant wave height. Wave height and wind speed are plotted in regards to their probability of occurrence in percentage [1].

5.2.3 Current data at COREWIND location

The influence of currents on the FOWT mooring system can be divided into wind-induced and tidal currents. Wind-induced currents are caused by winds above the water's surface, causing water to flow in the direction of the wind in the ocean's upper layers [1]. The velocity of this current depends on the intensity of the wind.

The current profile can be described by equation 1 below, as described in the COREWIND project by *Vigara et al.* [1].

$$v_{c,\text{ wind}}(z) = v_{c,\text{ wind}}(0) \cdot \left(\frac{d_0 + z}{d_0}\right) for - d_0 \leq z \leq 0 \tag{1}$$

In this equation, $v_{c,wind}(0)$ represents the wind speed measured at the reference height, d_0, for the depth at which the current velocity is determined, z. In addition to this wind-induced current, there is also the tidal current. It can be described by equation 2 as presented by *Vigara et al.* [**?**] in the COREWIND project.

$$v_{c,tide}(z) = v_{c,\text{ tide}}(0) \cdot \left(\frac{d+z}{d}\right)^{\frac{1}{7}} \text{ for } z \leq 0 \tag{2}$$

Here $v_{c,\text{ tide}}(0)$ represents the current velocity at the reference depth d. As in the previous equation, z represents the depth at which the tidal current is evaluated. Both equations were used to determine a total current based on water depth, shown in Figure 5. As presented, current velocity decreases with water depth, depending on the chosen profile.

The environmental data will not only serve for the later development of the load cases and the corrosion model but was also used for the dimensions of the wind turbine, the substructure, and the mooring system in the COREWIND project, which will be presented in the following chapters.

Depth (m)	Wind component (m/s)	Tidal component (m/s)	Total current speed (m/s)
0.00	0.57	0.49	1.06
-10.00	0.52	0.49	1.01
-20.00	0.48	0.48	0.96
-30.00	0.43	0.48	0.91
-40.00	0.39	0.48	0.87
-50.00	0.34	0.47	0.82
-60.00	0.30	0.47	0.77
-70.00	0.25	0.47	0.72
-80.00	0.21	0.46	0.67
-90.00	0.16	0.46	0.62
-100.00	0.11	0.46	0.57
-110.00	0.07	0.45	0.52
-120.00	0.02	0.45	0.47
-130.00	0.00	0.44	0.44
-140.00	0.00	0.44	0.44
-150.00	0.00	0.43	0.43
-160.00	0.00	0.42	0.42
-170.00	0.00	0.42	0.42
-180.00	0.00	0.41	0.41
-190.00	0.00	0.40	0.40
-200.00	0.00	0.39	0.39
-210.00	0.00	0.38	0.38
-220.00	0.00	0.36	0.36
-230.00	0.00	0.34	0.34
-240.00	0.00	0.31	0.31
-250.00	0.00	0.00	0.00

Figure 5: Current velocity near Gran Canaria. Wind-induced current [m/s] and tidal current[m/s] are plotted in regard to the water depth[m], resulting in a total current speed [m/s] [1].

5.3 Turbine details of the COREWIND project

The turbine used in the following experiments is an IEA 15 *MW* turbine. It has a cut-in wind speed of 3 m/s, a rated wind speed of 10.77 m/s, and a cut-out wind speed of 25 m/s. The turbine has a direct drive generator [18]. The rotor radius is 120m, and the hub height is 150m. In Figure 7, the pitch angle of the blades of the IEA 15 is plotted against the wind speed. This turbine is built on a three-column semi-submersible substructure, which will be described in the following chapter 5.4.

Figure 6: IEA 15 mounted on the semi-submersible floater [1].

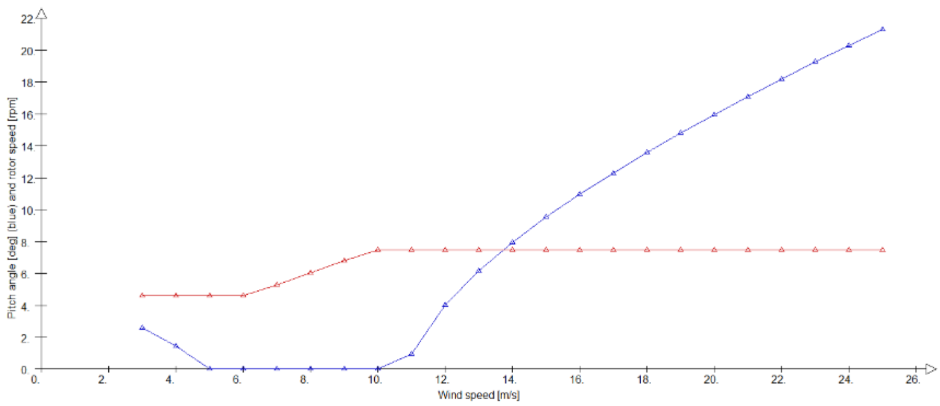

Figure 7: Controller function of the IEA 15. The pitch angle (blue) [degrees] and rotor speed (red) [rpm] are plotted against the wind spreed[m/s] [18].

5.4 Substructure details of the COREWIND project

The substructure used in the COREWIND project at the Gran Canaria site, a semi-submersible, is a pontoon-like structure. It is called ActiveFloat and was developed by COBRA [1]. It floats from 26 meters below the seawater line to 9 meters above. This can be seen in Figure 8. It is connected to three catenary mooring lines at 15 meters depth in an alignment of 120° to another, keeping the FOWT in place.

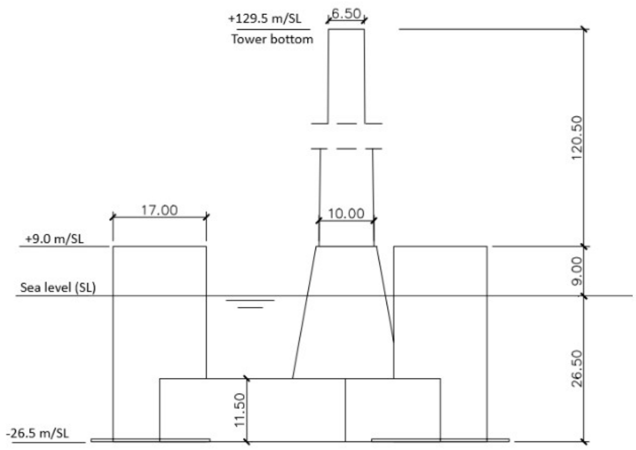

Figure 8: Side view of the semi-submersible floater in the dimensions of meters [1].

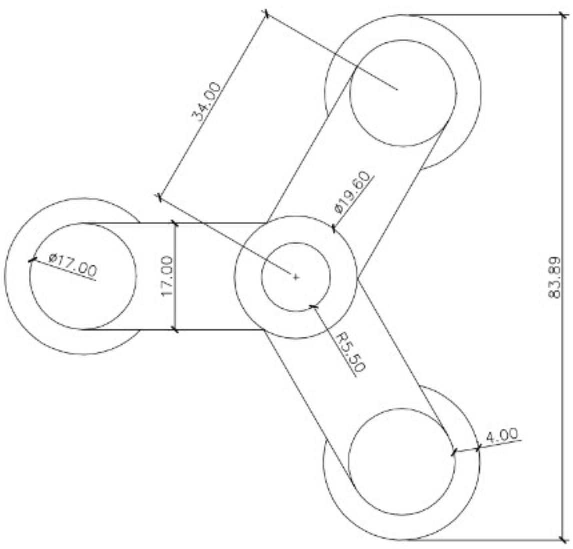

Figure 9: Top view of the semi-submersible floater in the dimension of meters [1]

.

5.5 Mooring line details of the COREWIND project

As described above, three mooring lines are connected to the FOWT. The mooring lines used in the following case study are catenary mooring systems made out of chains. These mooring chains are entirely made out of R4 mooring steel material. The properties of R4 are presented in the table below.

Material Name	**Mass density [Te/m^3]**	**Yield strength [GPa]**	**Poisson ratio**
R4	7.98	210	0.3

Table 6: R4 mooring steel material properties as presented by *Zarandi et al.* [19].

The utilized chain has a diameter of 160 mm with a total unstretched length of 614 meters [20]. As shown in Figure 10, a standard chain dimension length is six times the diameter, while the height is 3.35 times the diameter. The inner bend diameter has a radius of 0.6 times the diameter. A further factor that is dependent

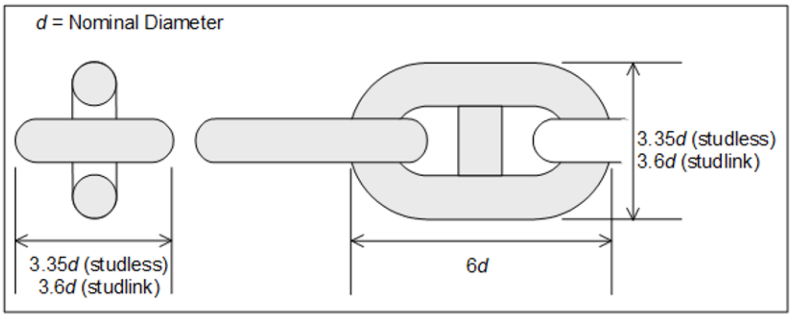

Figure 10: Mooring chain dimensions given in the IACS W22 report [21].

on the diameter is the minimum breaking load, which is calculated based on Equation 3 [6], in which d represents the diameter.

$$MBL = 0.0223d^2 * (44 - 0.08d) \tag{3}$$

5.6 Anchor details of the COREWIND project

Based on the seabed, it was determined in the COREWIND project that a drag-embedded anchor would be sufficient to anchor the FOWT and mooring system to the seabed [1]. The following work is based on a catenary chain interacting with loads and corrosion, so the anchor is not included in the analysis. This is based on the assumption that the catenary mooring line, shown in Figure 11, compensates for the floater's loads by lifting the chain on the seabed. Since a remaining part of the chain will, in an ideal case, always lay on the seabed, the anchor does not experience direct loads.

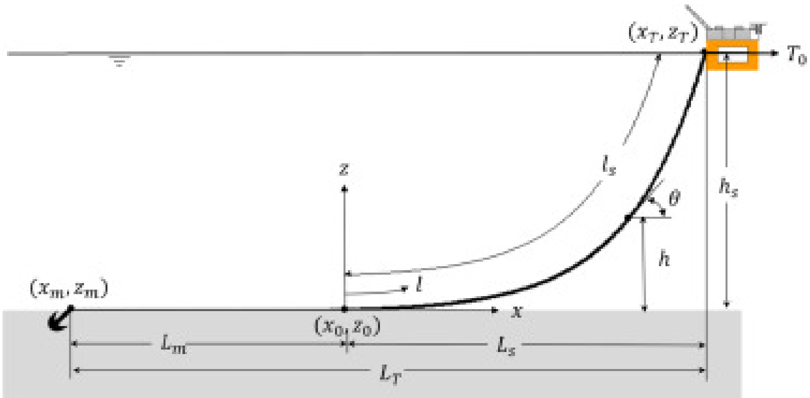

Figure 11: Catenary mooring line shape example based on a FPSO [6].

6 Methodology

A methodology was suggested in the literature review to answer the research questions. The flow chart is shown in Figure 12.

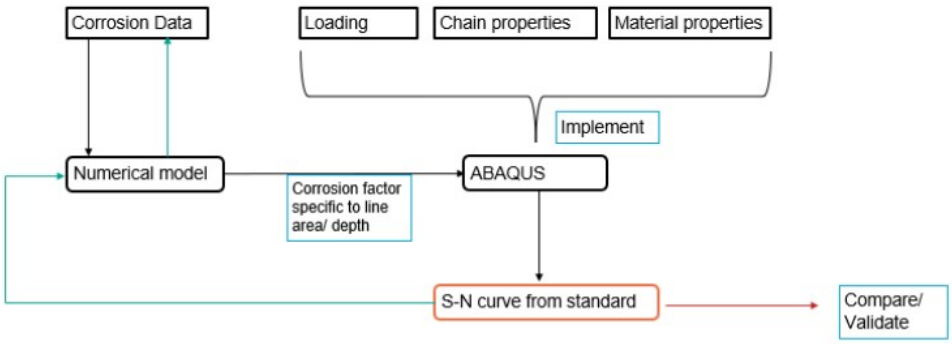

Figure 12: Flow diagram representing the methodology procedure.

The proposed methodology is divided into a step-wise procedure. In the first step, corrosion data, load cases, and material properties should be determined. An example floating project was identified to determine all the chain specifications and the chain details were extracted. Based on these details and the environmental loads, the load cases on the FOWT were then determined in the open source tool OpenFast to calculate the line loads on the mooring chains.

In the second step, a finite element modeling of different chain segments should be carried out in ABAQUS. In this model, the variables from the first step were to be implemented depending on the placement of the chain segments along the line. The finite element model was built as a half mooring chain based on the mooring chain details presented in chapter 5.5. Then, the loads from OpenFast in combination with a corrosion model based on *Nevshupa et al.* [7] and the Fickian model were implemented.

In the last step, the results were compared to current methods, and a validation was conducted. Here the results from the FEM were compared to another and the outputs from *Lone et al* [22]. The detailed methodology is presented in the following paragraphs.

6.1 Determination of the chain details

In order to model the chain accurately for later implementation in finite element methods, the chain segment dimensions had to be determined and drawn.
The standard for studless chains can be used to determine the chain dimensions, as shown in Figure 10 in chapter 5.5. Based on the diameter, the mooring chain segments were modeled using AutoCAD.

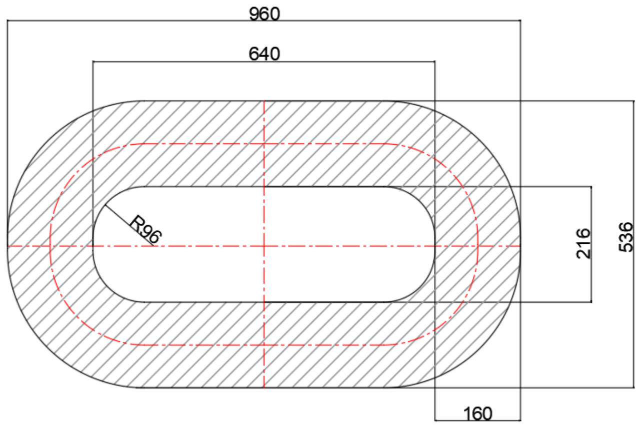

Figure 13: Side view of the mooring chain segment with the relevant dimension in millimeters for replicating the chain.

The chain diameter was also used to determine the equivalent diameter for later implementation in OpenFast. An equivalent diameter is utilized as OpenFast determines loads on a steel rod, representing the mooring chain. The equivalent diameter is 1.8 times the original diameter, resulting in an equivalent diameter of 288 mm.
The load cases presented in the following chapter were determined based on this equivalent diameter.

6.2 Determination of the load cases

To determine the loads modeled on the mooring lines, OpenFast was used. OpenFast is an open-source tool in which floating offshore wind turbine loads and the environmental conditions can be used to calculate forces and degrees of freedom (DOFs). A mooring system tool was required to combine the calculated forces and degrees of freedom calculation with a mooring system analysis. Multiple software can be utilized for this determination. One possible option was the MoorDyn analysis of OpenFast itself. Further, Orcaflex, FEAMooring, or MAP+ could be used. Some requirements were set up to choose the best tool for the desired outcome. First, the tool should be open-source so that the methodology can be replicated in the future without purchasing software. Further, the tool should be able to implement wave-kinematics, be reliable and validated through previous research. For the basis of the decision process, the paper published by *Wendt et al.*[23] was used. In this paper, *Wend et al.* compared the results of different mooring tools. A summary of these tools regarding the criteria can be found in Table 7. In conclusion, Orcaflex is not an open-source tool and can not be utilized. MAP+ did not suffice in the comparison by *Wend et al.*. And lastly, FEAMooring does not

Tool	MoorDyn	FEAMooring	MAP++	Orcaflex
Open source	Yes	Yes	Yes	No
Modeling approach	Lumped-mass Morrison equation	FEM	Quasi static	Lumped-mass
Includes	Mooring stiffness Inertia and damping forces Weight effects Buoyancy Seabed contact forces Hydrodynamic loads	Axial elastic stretching Axial structural damping Added mass Inertia loads Seabed contact Geometric non-linearities Buoyancy Hydrodynamic drag	Seabed friction Geometric- non-linearities Elastic stretching	Wave-kinematics Nonlinear effects Bending stiffness Torsional stiffness
Neglects	Bending stiffness Torsional stiffness Seabed friction	Line bending Torsion Seabed friction Line interconnections Wave kinematics	Dynamic line loads Line bending stiffness Three-dimension	Friction
Validation	Yes	Internal verification Not against wave tank	Yes	Yes

Table 7: Comparison of different mooring analysis tools to determine mooring dynamics [23].

include the calculation of wave kinematics.

These findings led to the decision to use the OpenFast tool MoorDyn for the Mooring analysis. MoorDyn is a lumped mass discretization and can be utilized to analyze the mooring system responses.

As mentioned in chapter 5, the utilized OpenFast model of the Activefloat wind turbine with a semi-submersible floater was published in the frame of the COREWIND project. This model already includes the main settings for the turbine, substructure, and mooring line. As OpenFast works with different Python modules as input for one main file, the specifics of the turbine, substructure, mooring systems, and environmental data are implemented in different modules. These modules, mainly used in the following analysis, are presented in Table 8.

Module	Description	Analysis specific constants	Analysis specific variables
AeroDyn	Aerodynamics	Blade properties Tower properties	-
ElastoDyn	Defining turbine specifics	Tower, Turbine and Hub dimensions	Rotor speed Pitch of the blades
HydroDyn	Aero-hydro-servo-elastic simulation	Current velocity	Wave height &direction Current Direction, Wave peak period
InflowWind	Processing of wind-inflow	Wind type	Wind speed Wind direction
MoorDyn	Defining mooring specifics	Chain properties	-
ServoDyn	Modeling options for the controller	Pitch control	-

Table 8: Utilized OpenFast files in the determination of mooring line loads [24].

Since multiple load cases had to be calculated, a Python script was developed based on the Python toolbox of OpenFast. This script made it possible to change the required variables in the modules to calculate the required load cases. The variables on which the script was based are:

- Wind speed
- Wind direction
- Wave height
- Wave peak period
- Wave direction
- Current direction

These variables were established using the environmental data presented in chapter 5.2. For the tidal current, the two main tide directions 22.5° and 202.5° were utilized as these are the dominant directions. A range of 0 to 68.5 radians was implied for the wind and 0 to 45 radians for wave direction. Therefore, all possible wind directions were considered, which had a higher probability. It was reasoned that even though the probability that maximum loads can occur from other wind or wave directions is low, the probability that it occurs over the lifetime is very small and, therefore, can be neglected. Further, the wind direction was also implemented as the direction of the wind-induced current. Based on the wind direction, the wave height and peak period were implemented as presented in Table 5 and Figure 4. As a basis, the wind speed was implemented in a range from 0 to 25 meters per second for each combination of environmental loads.

Parts of the environmental data were implemented as constants, like the current profile in depth and the mooring line data. A list of these steady inputs, their respective implementation module, and their name are presented in Table 9.

Environmental constant	Module	Constant Name	Constant value
Steady wind	InflowFile	WindType	1
Current velocity tide	HydroFile	CurSSV0	0.49
Current velocity wind	HydroFile	CurNSV0	0.57

Table 9: Constant values implemented in OpenFast.

The constant values in Table 9 for the currents represent the current velocity at reference depth. With this current velocity, the velocity at any depth can be calculated in OpenFast using the equation shown in chapter 5.2. Equation 1 determines the current induced by wind influence. Equation 2 is used to determine the velocity of the tidal current.

The final output of the OpenFast calculation can be defined based on the required analysis. In this process, several outputs were generated, mainly related to the mooring analysis. The output file .MD.out and the .out file were used for this.

Open Fast outputs a time series with the corresponding variables in these files. The time series of the Farilead outputs, set to 20 minutes, as well as the loads along the mooring line, were analyzed using a damage equivalent load (DEL).

DELs are calculated using the Rainflow-counting method. Rainflow-counting is used to determine fatigue from load histories. It counts load cycles in load histories in terms of the number and amplitude of cycles.

The equation for the determination of the DEL is given in equation 4.

$$S_{DEL} = \sqrt[m]{\frac{1}{N_{raf}} \sum n_i \times S_i^m} \tag{4}$$

In this equation N_{raf} represent the reference cycle number, m is the S-N curve slope , and $n_i$and L_i give the cycle and the amplitude of load respectively [25]. In the further analysis, the slope of the S-N curves is set to 4 according to *DNVGL-RP-C203* [26]

6.3 Determination of the corrosion model

The corrosion model used in this project was based on the findings of *Nevshupa et al.* [7]. As can be seen in Figure 14, *Nevshupa et al.* developed a method to determine the corrosion rate of R4 mooring steel based on temperature and oxygen in synthetic seawater with a salinity of S35. To determine the rate regarding the specific location of the COREWIND project, temperature and oxygen data of the world ocean atlas were utilized. The data utilized from the World Ocean Atlas has the code 38589 and was gathered in February of 2020 [27]. The data is presented in Table 10. Even though the location of the extracted data is at a distance of 14 km from the COREWIND project, the map in Figure 15 shows that the difference in distance is negligible. Based on this data, the corrosion rate in depth was determined and can be seen in Figure 16. The corrosion rate decreases as the oxygen and temperature decrease with water depth. This data will be utilized in the later corrosion analysis along the mooring line.

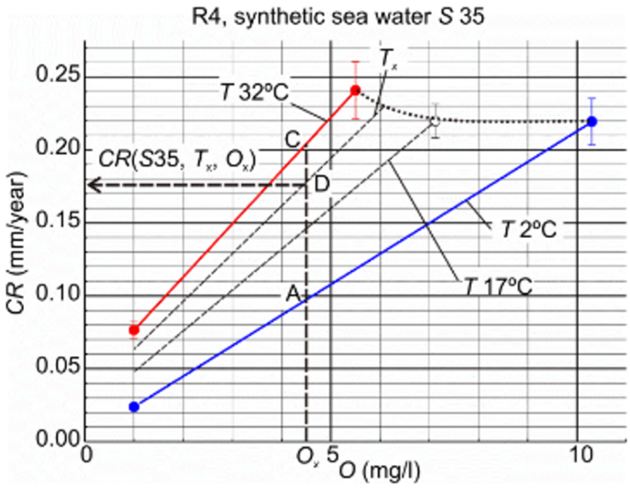

Figure 14: Corrosion rate based on oxygen and temperature developed by *Nevshupa et al* [7].

Units	Depth [m]	Degrees[C]	Salinity [PSS]	Oxygen [umol/kg]	Oxygen [mg/l]
1	0.00	18.3874	36.6210	231.6	7.4112
2	5.00	18.3883	36.6211	231.6	7.4112
3	10.00	18.3896	36.6209	232.4	7.4368
4	15.00	18.3899	36.6209	233.3	7.4656
5	20.00	18.3911	36.6210	233.3	7.4656
6	25.00	18.3922	36.6210	233.5	7.472
7	30.00	18.3932	36.6211	233.3	7.4656
8	35.00	18.3941	36.6211	233.7	7.4784
9	40.00	18.3949	36.6210	233.2	7.4624
10	45.00	18.3953	36.6208	233.7	7.47848
11	50.00	18.3958	36.6205	233.6	7.4752
12	55.00	18.3960	36.6201	233.0	7.456
13	60.00	18.3927	36.6197	233.1	7.4592
14	65.00	18.3697	36.6151	232.3	7.4336
15	70.00	18.3204	36.6055	230.4	7.3728
16	75.00	18.2969	36.6017	229.8	7.3536
17	80.00	18.1949	36.5845	228.1	7.2992
18	85.00	18.1185	36.5728	225.1	7.2032
19	90.00	18.0080	36.5565	223.4	7.1488
20	95.00	17.9779	36.5522	223.2	7.1424
21	100.00	17.7795	36.5057	215.5	6.896
22	125.00	16.9974	36.3635	200.4	6.4128
23	150.00	16.4602	36.2847	198.5	6.352
24	175.00	16.0840	36.2290	189.7	6.0704
25	200.00	15.7814	36.1828	185.1	5.9232

Table 10: Temperature and Oxygen data extracted from the WOA in regards to the location of the COREWIND project [27].

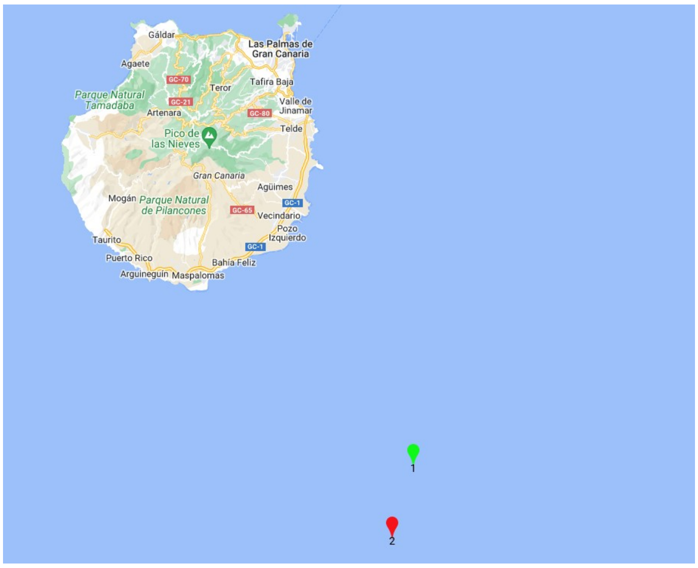

Figure 15: Distance between the location used by *Vigara et al.* and the extracted data location. The green market point with number 1 represents the actual COREWIND location. The red marker number 2 represents the location where the data was extracted.

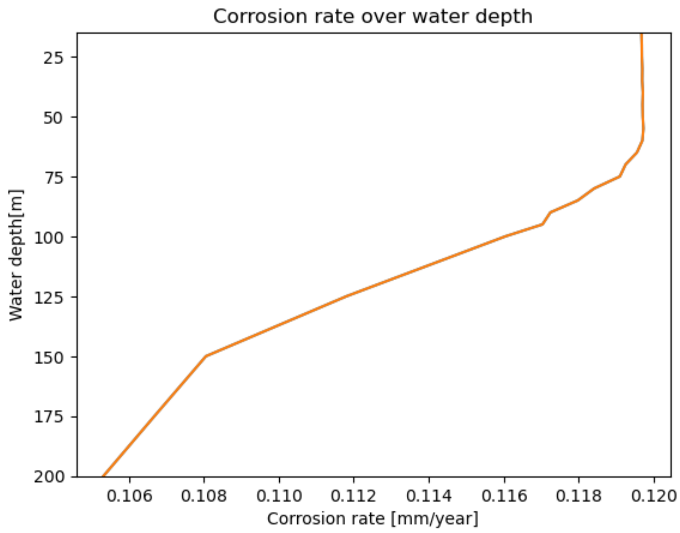

Figure 16: Corrosion rate in regards to water depth based on the data of the WOA and the model by *Nevshupa et al.*.

While this model only represents the corrosion initiation in the first year and does not imply the corrosion development over the whole immersion time, it was modified with a long-term immersion model. In Figure 17, three models for corrosion of long-term immersion are compared.

One is the power law, which is shown in equation 5. This equation gives the corrosion rate R in [mm/year] based on the corrosion factor C, calculated by the above corrosion over depth model, and the time in years represented by t.

It was presented by *Melchers et al.* [28] that if b is set to 0.5, it is a purely Fickian diffusion. To compare the Fickian diffusion to a higher power, another curve based on the power law was plotted with an exponent equal to 0.8. The third model is a simple linear model, assuming the corrosion rate does not decrease based on corrosion products after the first year, as included by Fickian.

$$R = C * t^b \tag{5}$$

The plot shows that the corrosion rate per year increases as the exponent b increases. The linear model also gives the highest overall corrosion rate as it does not consider any slowing of corrosion. This model is not recommended as corrosion slows down during development, with corrosion products acting to protect the steel.

Based on this comparison, it was decided to implement the Fickian corrosion model. As this corrosion model is used in other research, the comparison of results is simplified by this assumption. Corrosion will be applied in the finite element model as corrosion pits, depending on which section is modeled on the water depth and immersion time. The corrosion pits will have a pit depth of the corrosion rate calculated based on the Fickian model with the exponent 0.5.

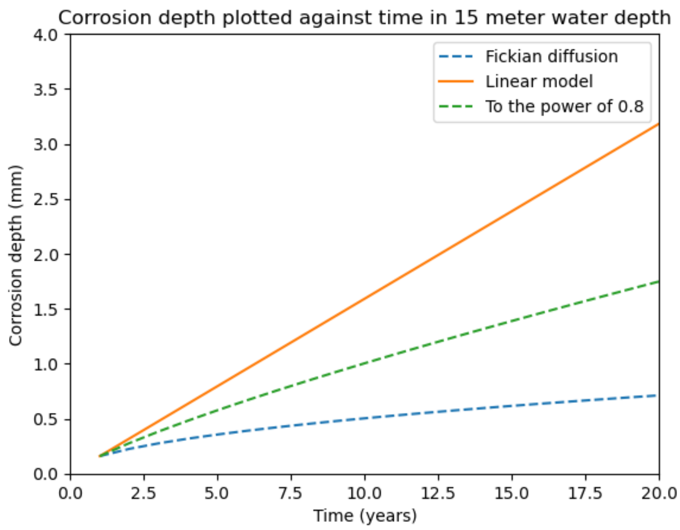

Figure 17: Comparison of long-term corrosion immersion models.

6.4 Determination of the finite element analysis

For the finite element analysis, ABAQUS is used to model the different sections along the mooring line under the respective tensions. Finite element models use the body of a given structure in combination with material properties, boundary conditions, and many other unique features to calculate the impact of loads on the body. They can be helpful in many areas of engineering, as no experimental setup is needed, and several tests can be executed.

In the following experiments, a finite element model based on the mooring line of a floating wind turbine was used to determine the stresses in the chain and, consequently, fatigue life. Different models were tested regarding running time, appropriate representation, and modeling accuracy to determine the correct representation for such a chain. Even though it would be easier to model a whole mooring chain and then develop a corrosion model to gain the load distribution along the chain, the run time of this approach would not be suitable for the given time frame. Therefore, a simple model was used with a short running time.

A model was developed based on the hot spot analysis, executed by *Lassen et al.* [29], in which the stress in the mooring chain is analyzed in the hot spot region of the bend of the mooring line. Using finite element methods, this is a standard procedure to determine the fatigue life of chains. In the following paragraphs, the exact utilized model is presented.

6.4.1 Development of the finite element model

First, the model was created in the parts section of ABAQUS based on the dimensions of the mooring chain determined in chapter 5.5. The side view of the mooring chain is shown in figure 18. It was developed in the so-called path sketch in ABAQUS. In the path sketch, the side view of the center line of the mooring chain was drawn. Using the sweep function, this center line is utilized to make a 3D model out of the 2D model. The sweep function utilizes the diameter of the path, presented in Figure 19, and sweeps it along the center line .

The quarter chain was split into the upper and lower half during modeling, making it possible to apply the load on the chain in the later modeling stage only on the inside. After closing both of these sketches, a solid model is developed by ABAQUS, presented in Figure 20. A sweep path for the upper half was developed along the same path sketch, and thus, the upper half was determined, shown in Figure 21. These two counterparts were combined into a quarter chain in the Assembly module of ABAQUS. Subsequently, this quarter chain was combined with a mirrored counterpart into a chain half as presented in Figure 22. The half-chain model was then used in all the ABAQUS modules regarding properties, load, boundary conditions, and mesh size.

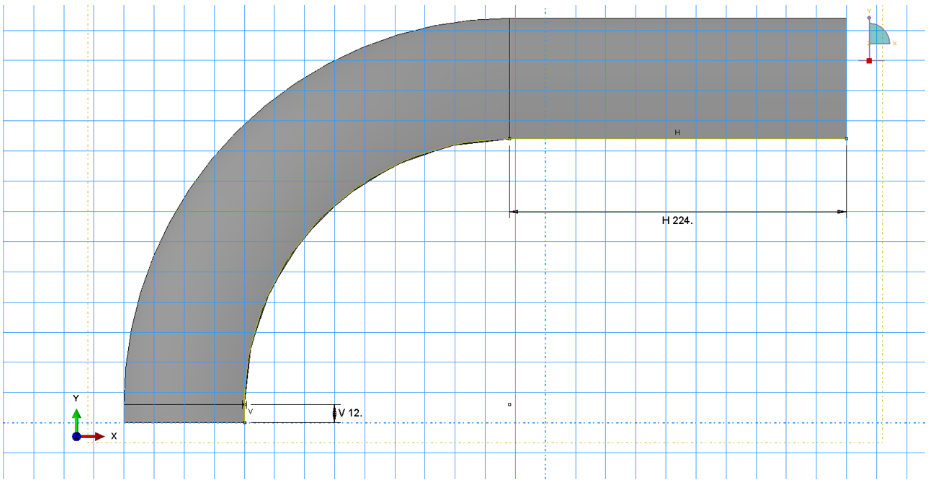

Figure 18: Side view of the mooring chain quarter in ABAQUS, with the dimensions based on the mooring chain standard.

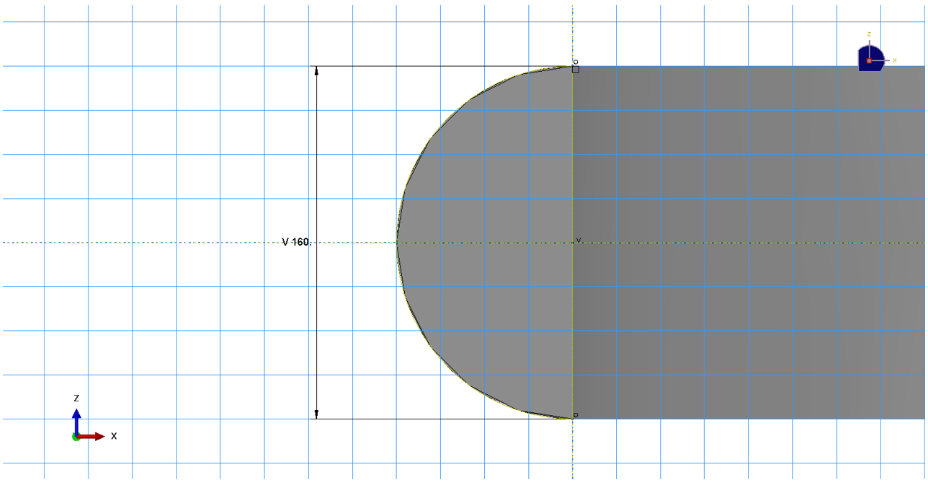

Figure 19: Plane view of the mooring chain quarter in ABAQUS, with the dimensions based on the mooring chain standard.

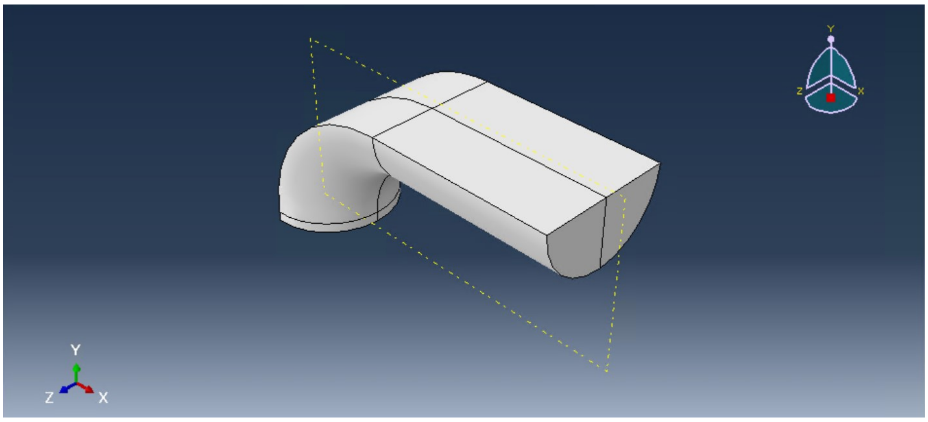

Figure 20: Developed part combined from the side and plane view in ABAQUS.

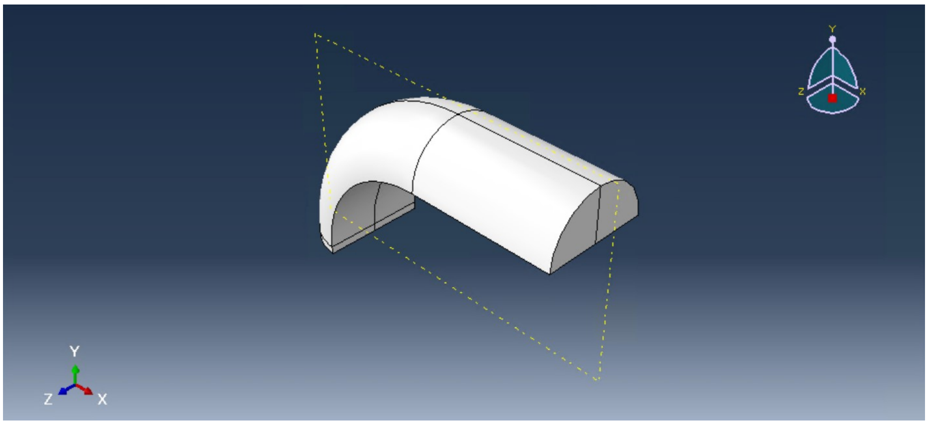

Figure 21: Developed upper part combined from the side and plane view with a change of the diameter on the plane view in ABAQUS.

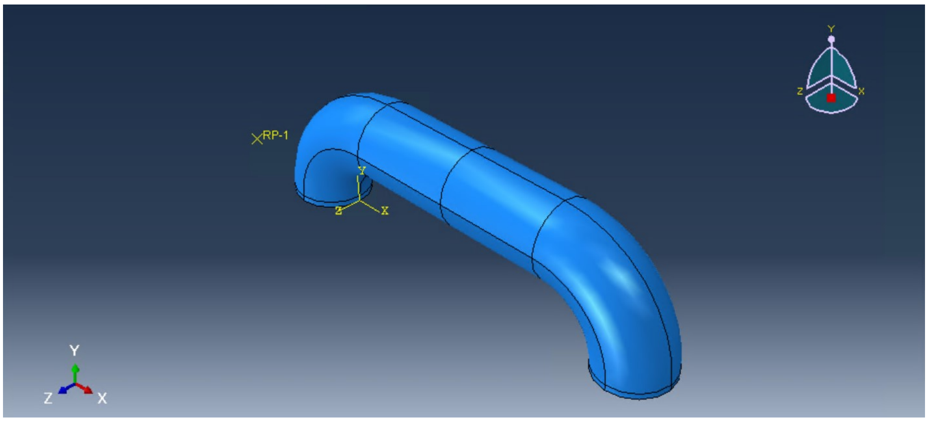

Figure 22: Half mooring chain used in the further models in ABAQUS.

6.4.2 Definition of material properties in the finite element analysis

A material was defined in ABAQUS to match the properties of R4 mooring steel as described in chapter 5.5, but using the units of ABAQUS. The results, which can be seen in Table 11, were then assigned to the section of the mooring chain half. Additionally, the plastic deformation properties of R4 mooring steel were applied to the model based on the monotonic curves for R4 presented in Figure 23 by *Zarandi et al.*.

Material Name	Mass density[Te/mm^3]	Yield strength[MPa]	Poisson ratio
R4	7.98E-9	210000	0.3

Table 11: Material properties utilized in ABAQUS with the units depending on a ABAQUS sketch basis in millimeters.

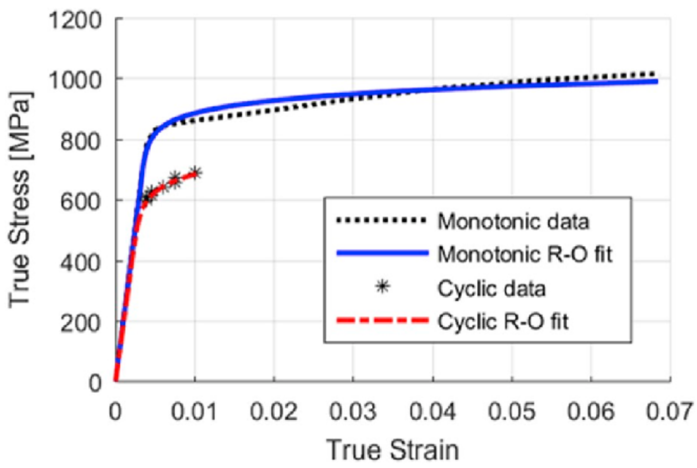

Figure 23: Plasticity properties of R4 mooring steel determined by *Zarandi et al.* [30].

Yield Stress[MPA]	Plastic strain]
800	0
841.7910448	0.005691057
862.6865672	0.01001626
895.5223881	0.02003252
934.3283582	0.030162602
967.1641791	0.040292683
988.0597015	0.050081301
1008.955224	0.060097561
1017.910448	0.067609756

Table 12: Plastic property of the mooring steel by *Zarandi et al.* [30].

6.4.3 Determination of coupling in the finite element analysis

In order to apply loads to the model, a reference point was implemented with coupling to the inner parts of the mooring chain model. The coupling allows a load to be applied to a reference diameter on the inner bend, similar to the force of another mooring chain segment acting on the model. A coupling study was executed to determine the correct implementation of the force, similar to the real model. This coupling study found that the maximum stress does not change with varying diameters if the connection points are positioned on the model part's surface. Based on this result, a coupling diameter of 400 mm was chosen.

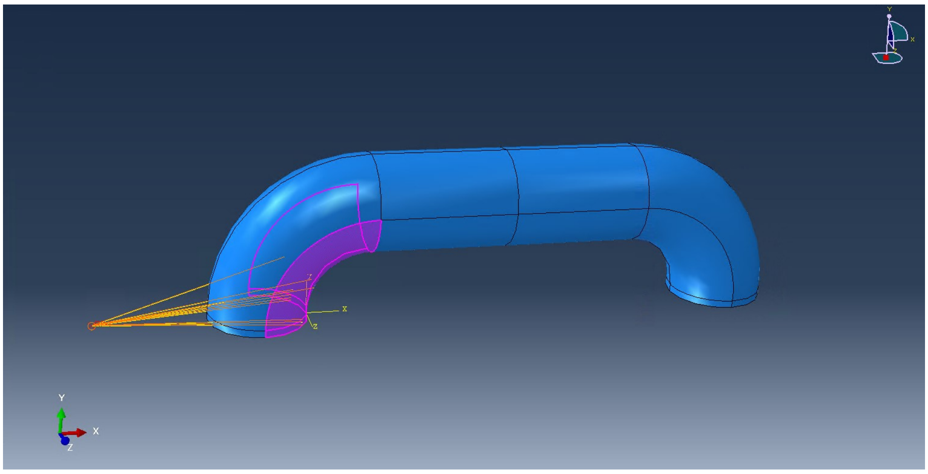

Figure 24: Coupling between the reference point and the mooring chain model.

6.4.4 Determination of boundary conditions in the finite element analysis

Boundary conditions had to be applied to the model to constrain the chain in place and apply loads. The side of the half-chain model opposite the load was fully constrained in all directions, similar to the side where another chain holds the mooring chain. On the side of the mooring chain where the loads will later be applied, a boundary condition is applied as a symmetries constraint. Symmetrical constraints resemble the other half of the mooring chain, which is not modeled. It behaves similarly to the other half of the mooring chain but still allows the chain to move in the x-direction of the load. Figure 25 gives an example of how the boundary determination looks. The reference point is also constrained according to symmetrical constraints, and the load is applied in the x-direction and y-direction. The OpenFast load in the z-direction here is translated to the y-direction as the direction of the mooring chain regarding the axis system changes.

6.4.5 Determination of load application in the finite element analysis

A load is applied to the reference point to implement the equivalent loads calculated by OpenFast on the mooring chain.

The applied force is presented in the next chapter, where the results of the OpenFast module are presented. From the OpenFast equivalent loads, only half of the load in each direction was applied, as the FEM was conducted utilizing only half of a chain segment. The hydro static pressure is also applied to the entire

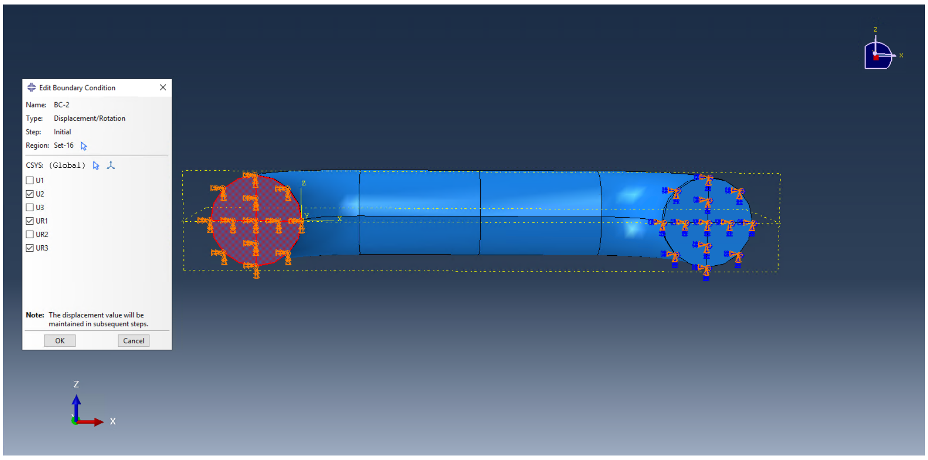

Figure 25: Boundary conditions of the ABAQUS model on the site of the mooring chain on which the load is applied.

mooring chain, as seen in Figure 26. The pink arrows resemble the hydro static pressure. Hydro static pressure depends on the water depth and is described by the corresponding Equation 6 [31].

$$P = \rho * g * d \tag{6}$$

In this equation, P represents the hydro static pressure, ρ represents the density of the seawater, which can be assumed to be $1025 kg/m^3$, and lastly d is the water depth .

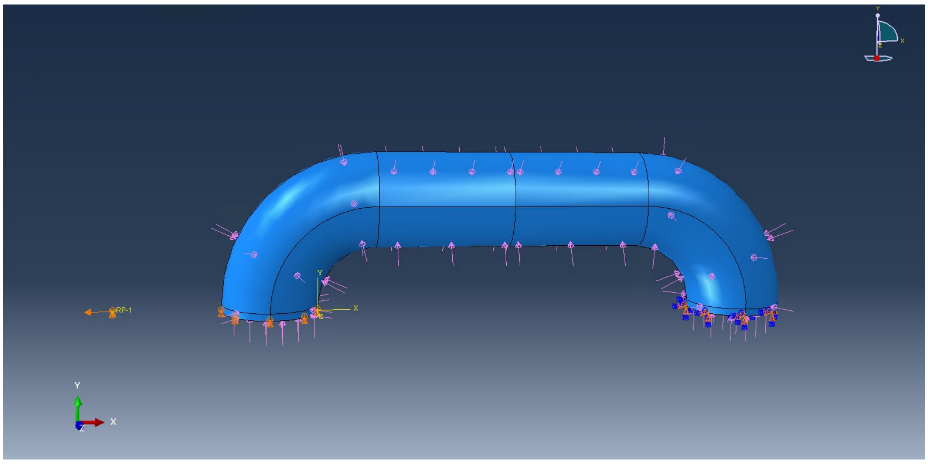

Figure 26: Hydro static loads on the ABAQUS model represented by the pink arrows normal to the mooring surface.

6.4.6 Determination of the utilized mesh in the finite element analysis

A mesh was created in ABAQUS to create the finite elements over which the stresses are analyzed. A mesh sensitivity study was conducted to determine the appropriate mesh size for analyzing the mooring chain. The

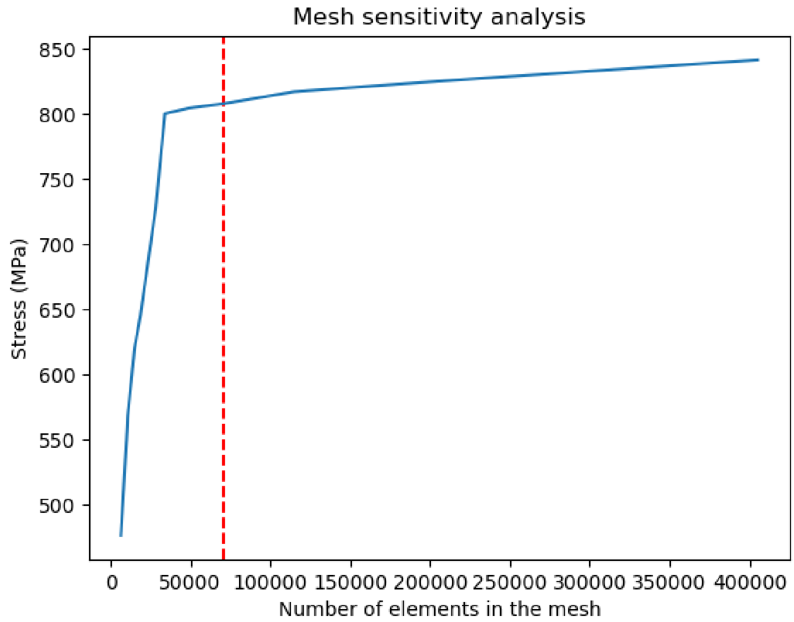

Figure 27: Mesh sensitivity study of the ABAQUS model based on the element number and size of displacement. The red dashed line indicates Mesh size 7, which was chosen.

result is shown in Figure 27. Although a finer mesh can result in more detailed results, the computation time increases as the mesh's size decreases. Therefore, a compromise was made, and a mesh size of a hexagon-shaped 7 mm was selected, indicated with the red line. This size best compromises a precise result and acceptable computation time. The final mesh model is presented in Figure 28.

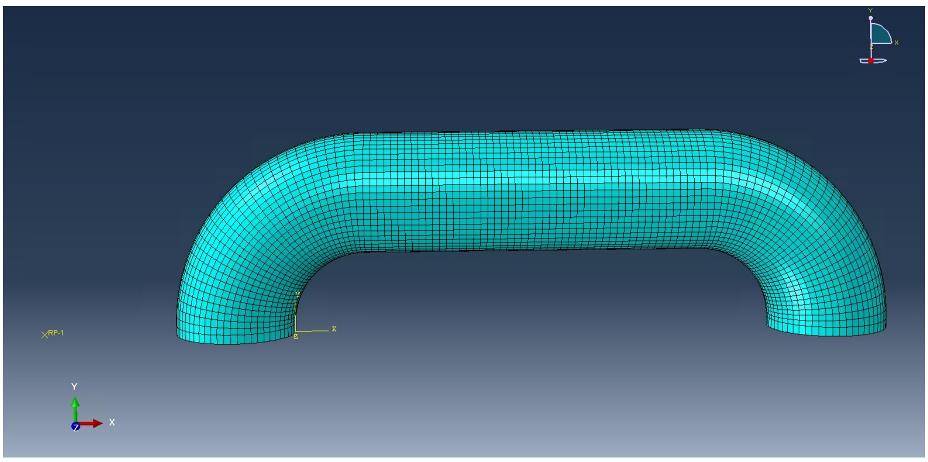

Figure 28: Mesh representation of the ABAQUS model.

6.4.7 Determination of the corrosion implementation in the finite element analysis

Corrosion is implemented in the finite element model as a corrosion pit based on a corrosion rate interpreted as a reduction in diameter. One pit is implemented per model at critical locations for crack initiation in the model. The locations are shown in Figure 29. In order to implement the corrosion model, the mesh had to be adjusted in these areas, otherwise, the mesh would not be sufficient to analyze the exceptional curvature of the pit. After conducting a second mesh convergence study, a tetrahedral mesh with a size of 0.15 was chosen. The corrosion pit was based on the model, immersion time, and its location in the water column.

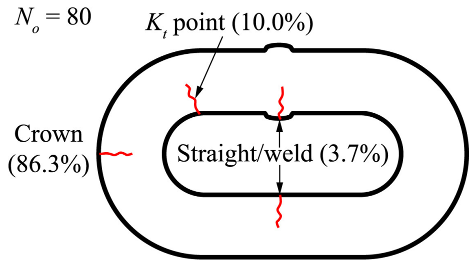

Figure 29: Most prominent locations for the development of fatigue cracks on the mooring chain segment found by *Mendoza et al.* [11].

6.5 Fatigue analysis

Fatigue life results are based on the analysis of stresses occurring in a model based on S-N curves. These curves estimate the number of cycles a model can withstand under a range of stresses that occur in the model. S-N curves are given in standards, but further research has been carried out to determine S-N curves based on factors other than just material, for example, average load and corrosion. Lifetime determination based on S-N curves through a stress range is given by the Equation 7 describing the S-N curve.

$$\log N = \log(a) - m\log(\Delta\sigma) \tag{7}$$

In this equation, $\log(a)$ represents the intercept parameter of the curve, m is the slope of the S-N curve, and $\log(\Delta\sigma)$ represents the logarithm of the nominal stress range. The parameters $\log(a)$ & m depend on the curve used for fatigue analysis. The nominal stress range can be calculated by Equation 8

$$\Delta\sigma = \sigma_{max} - \sigma_{min} \tag{8}$$

As σ_{min} can also be described as $R * \sigma_{max}$, the equation which will be analyzed in the fatigue determination is presented in Equation 9.

$$\Delta\sigma = \sigma_{max} - R * \sigma_{max} \tag{9}$$

Here, R is chosen based on the curve that is utilized. In the following S-N analysis, a $R = 0.1$ was chosen.

Three research methods are presented below, which will be used in the later service life analysis. S-N curves that can determine the service life of mooring chains are those presented in DNVGL-RP-C203[26]. This standard provides a wide range of S-N curves in air and seawater, with cathodic protection or free corrosion. The standard covers different materials and shapes, such as flat materials and tubular joints. For the analysis of R4 material mooring chains, the B1 curve in seawater with cathodic protection was chosen. The B1 curve represents rolled sections such as the mooring chain. The S-N curve for B1, taken from the standard, is shown in Figure 30 for seawater with cathodic protection of the steel. Figure 31 presents the S-N curve in the air. Here, the materials are presented regarding lifecycles under stresses in seawater with cathodic protection.

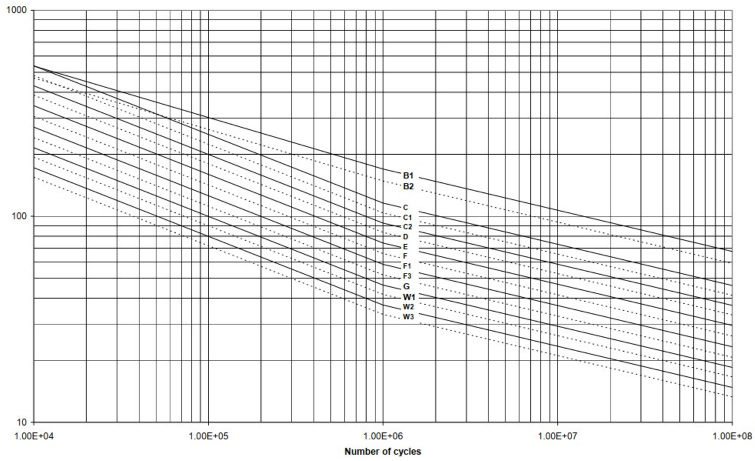

Figure 30: S-N curves in seawater under cathodic protection given by *DNVGL-RP-C203* [26].

The B1 curves give the $\log(a)$ and m parameters assumptions. It is divided by the lifecycle range analyses. The range of 10^7 cycles occurs up to a fatigue limit of 106.97 MPA. Therefore, everything equal to or below 106.97 MPA is analyzed using the parameters $m = 5$ and $\log(a) = 17.146$. The life cycles for the nominal stress ranges above 106.97 MPA are determined using $m = 4$ and $\log(a) = 14.917$.

The second curve utilized was given for B1 material in air. In this curve, the range of 10^7 cycles also occurs up to a fatigue limit of 106.97 MPA. Therefore everything equal to or below 106.97 is analysed using the parameters $m = 5$ and $\log(a) = 17.146$. The life cycles for the nominal stress ranges above 106.97 MPA are determined using $m = 4$ and $\log(a) = 15.117$.

The third curve used in the analysis of the models, which includes corrosion, is the B1 curve under the assumption of free corrosion in seawater. In this curve $\log(a) = 12.436$ and $m = 3$. In Figure 32, these curves are plotted, and it is evident that the free corrosion curve crosses the corrosion protection curve when the nominal stress range is greater than 300 MPa. This representation is misleading as steel, including corrosion protection, should not have a shorter life than steel without corrosion protection at any stress. Consequently, the free corrosion curve has been adjusted in accordance with the S-N curve for tubular joints in the standard. This resulted in a value of m=4 and a $log(a) = 14.73$ value with respect to the cathodic protection value. In the following analysis, the nominal stress ranges are plotted in regards to the parts of the presented S-N curves which are according to a number of cycles smaller than 10^7. This is based on the assumption made regarding the slope in the equivalent load calculation.

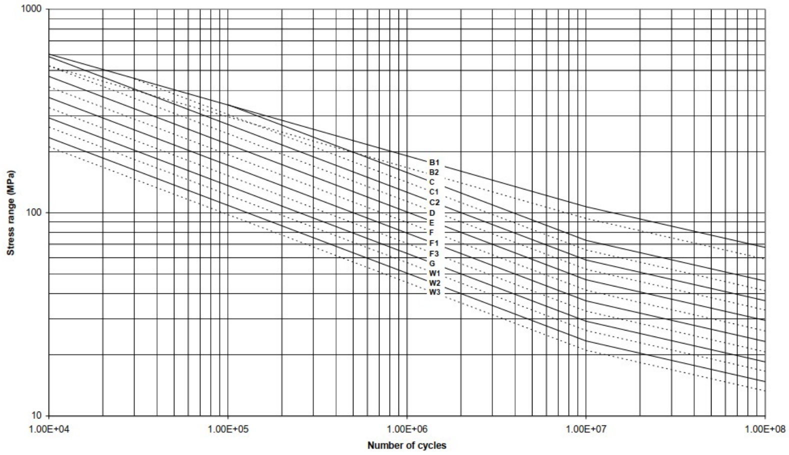

Figure 31: S-N curves in air given by *DNVGL-RP-C203* [26].

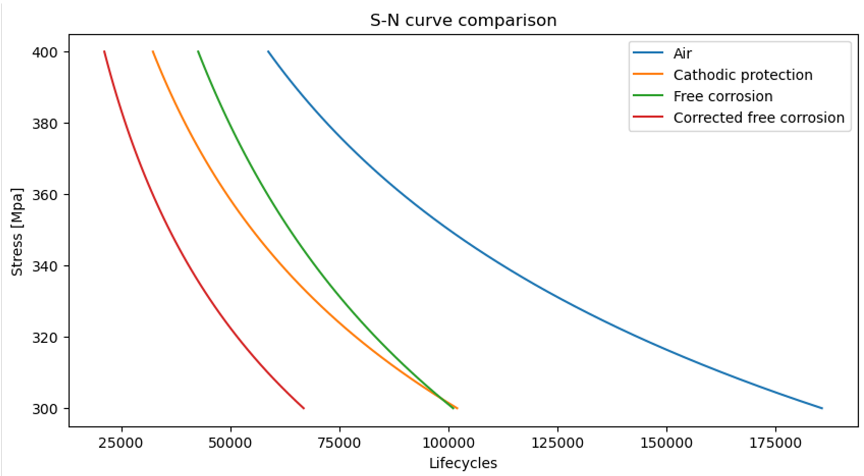

Figure 32: S-N curves comparison [26].

7 Numerical results and evaluation

The following sub-chapters present the results of the calculations based on the methodology presented. Firstly, the results of the OpenFast calculations of the COREWIND project of the turbine, substructure, and mooring system described in chapter 5 are given for the environmental conditions of the environmental data presented in the case study in chapter 5.2.

Subsequently, the results of the corrosion model and the OpenFast analysis were implemented in the finite element model in ABAQUS presented in chapter 6.4.1. Several models based on the load cases and corrosion evolution were calculated and compared using S-N curves as described in chapter 6.4.1.

7.1 OpenFast Results

The COREWIND model was implemented in OpenFast to determine the tension on the mooring chain. An OpenFast database provided by the COREWIND project was used to determine the loads on the fairlead sections. Based on the methodology explained in chapter 6.2, a wide variety of load cases were implemented to get an image of the loads the mooring system has to endure.

7.1.1 Determined loads

To analyze the results, the last line of the output file ".Md.Output" of each output was included in a summary file. This last row represents the residual loads from the applied load case at each fairlead and anchor. The summary file, therefore represents the most prominent at each fairlead and anchor based on the environmental data. A statistic of this summary file can be seen in Table 13.

	Fairlead 1	**Fairlead 2**	**Fairlead 3**	**Anchor 1**	**Anchor 2**	**Anchor 3**
count	4.627E+03	4.627E+03	4.627E+03	4.627E+03	4.627E+03	4.627E+03
min	2.28E+06	1.92E+06	1.95E+06	1.49E+05	1.13E+06	1.15E+06
max	3.89E+06	2.52E+06	2.77E+06	3.07E+06	1.71E+06	1.94E+06

Table 13: Results of the OpenFast calculations given as tensions in MN.

In Table 13, it can be observed that the highest loads occur in the first mooring line. Throughout the further analysis, the main focus will be on the tensions of Fairlead 1. Following this, the tension along the mooring line will be presented, which will be implemented in the later ABAQUS model.

7.1.2 Tension model along the mooring line

The OpenFast mooring dynamic model output was used to determine the stress distribution and compare it with the later fatigue distribution along the mooring line. It can further output each node location, leading to the shape of the mooring line as displayed in Figure 33. This data can be used to check the mooring line behavior, for example, the determination of the lift of the point from the seabed.

Further mooring line shape is also used to determine the angle of the mooring line between two nodes. This angle can then be used to calculate the out-of-plane bending of the chain segments. The tension at the node can then be implemented in the later model in x- and z-direction according to the mooring line angle. The tension part in the y-direction is hereby neglected, as it is insignificant compared to the other two directions. The previous results were just a mean of the time series to give the reader an impression of the magnitude and

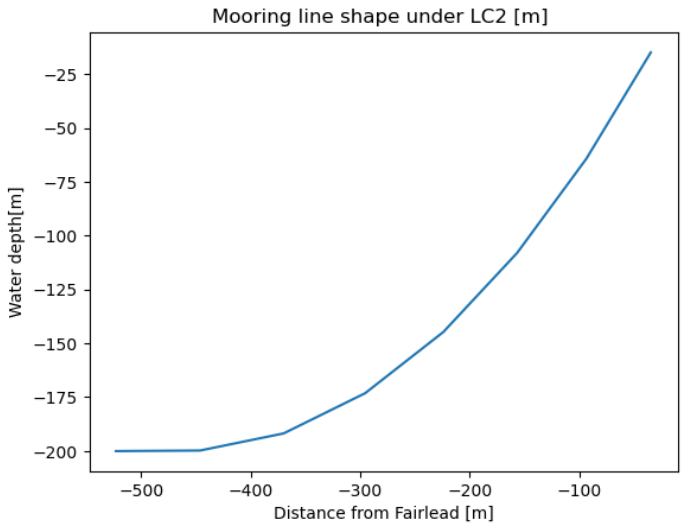

Figure 33: Mooring line shape based on a Fairlead tension of 3.06MN.

distribution of mooring chain tensions. To analyze the stresses within the chain, the most probable equivalent loads were applied to the model described in chapter 6.4.1. Additionally, in the following presented results, the loads are given as DEL so that the whole time series of 20 minutes is represented.

7.2 Finite element model results

To investigate the impact of different load cases along the mooring line in regard to the previous results of the OpenFast model, different mooring sections were modeled.

Three sections of the mooring line were identified where specific loads and corrosion rates should be applied. One was located close to the Fairlead. The second section was located in the middle of the water column at a depth of approximately 100 meters. A third section was set close to the seabed.

Due to the shape of the mooring line, these locations were not always on the same section of the line. So before implementing a FEM, each mooring line shape was calculated to determine the loads, angles, and exact locations of the representative nodes. In the following analysis, equivalent load calculations of the most probable loads were executed and implemented in the finite element analysis. In the Table below the chosen load cases are presented.

Load case	Wind speed [m/s]	Wind Direction [rad]	Wave Height [m]	Wave peak period [s]	Wave Direction [rad]	Current Direction [rad]
One	4	25	1.5	6	1	22
Two	4	25	1.5	7	1	22
Three	4	25	1	6	1	22
Four	4	25	1	7	1	22
Five	5	25	1.5	6	1	22
Six	5	25	1.5	7	1	22
Seven	5	25	1	6	1	22
Eight	5	25	1	7	1	22
Nine	6	25	1.5	6	1	22
Ten	6	25	1.5	7	1	22
Eleven	6	25	1	6	1	22
Twelve	6	25	1	7	1	22

Table 14: Load cases with a high probability of occurrence utilized to determine the difference in lifecycles.

These presented load cases have the highest probability of occurrence, according to the COREWIND data. All of them were executed with a number of 3 seeds. In Figure 34, the results of all the calculations of the different Load cases and seeds are presented. In the further analysis, Seed 2 was utilized for the analysis. To test the behavior of the mooring chain and possible corrosion locations, two chosen load cases are presented. Later on, a study of the most probable loads is executed to determine possible weak points along the mooring line.

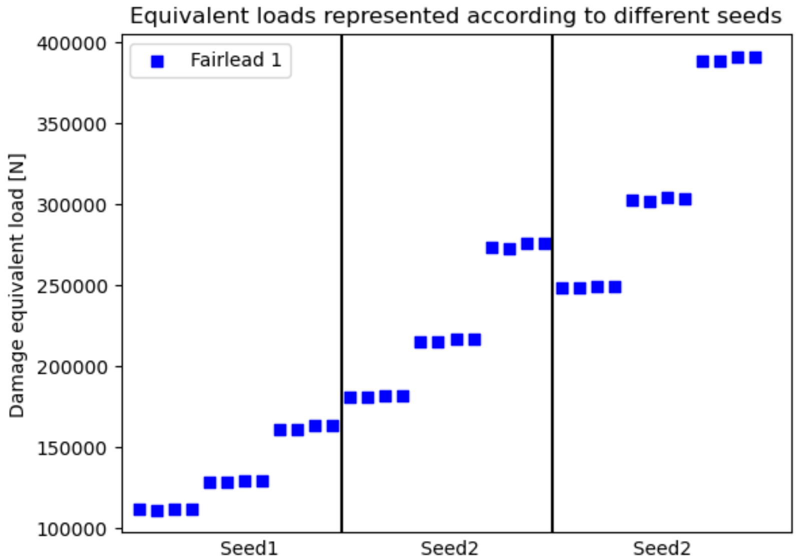

Figure 34: Most probable load cases and their equivalent loads according to Fariled 1

Model	**Section**	X-Location	Z-Location	**Equivalent load [KN]**
Model 1	Upper mooring line	-43.14	-20,2	180.427
Model 2	Middle mooring line	-163.3	-115.6	181.698
Model 3	Lower mooring line	-377.4	-196	190.046
Model 4	Upper mooring line	-41.13	-19.26	215.585
Model 5	Middle mooring line	-163.5	-111.9	219.149
Model 6	Lower mooring line	-377.6	-193.4	226.047

Table 15: Presentation of Load cases 2 and 6 utilized in the mooring analysis.

7.2.1 FEM results

The DELs and corrosion pits applied to the FEM model resulted in stresses in the model. An example result of the model is shown in Figure 35. As previously described, hot spot analysis was used during the ABAQUS analysis. This determined that the point of highest stress should be in the inner bend of the mooring chain segment, as seen in the model. The stresses seen are given as von Mises stresses, taking into account yielding.

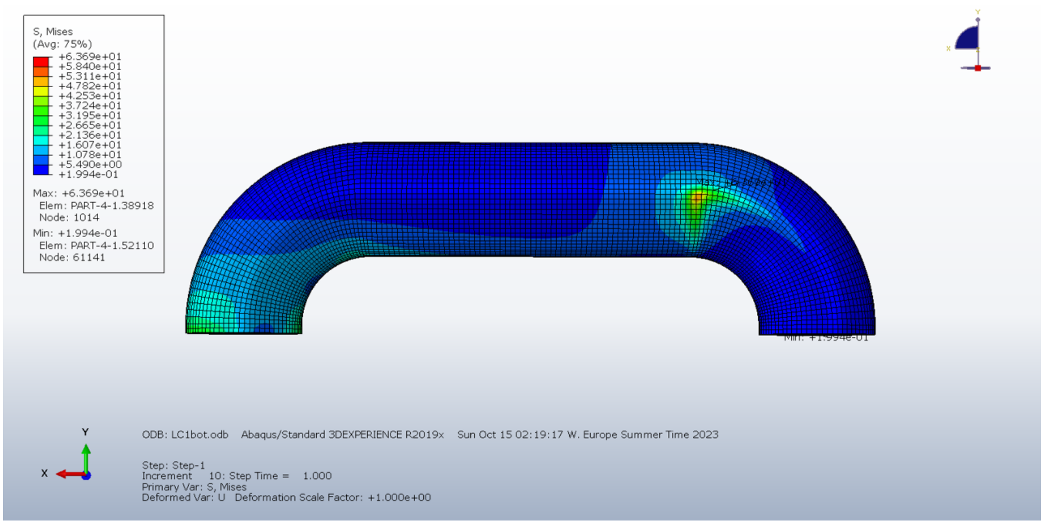

Figure 35: Resulting stresses in the half mooring chain of the mooring line.

7.2.2 FEM model without corrosion implementation

To determine the impact of corrosion on the lifetime, first corrosion-free models had to be determined. Based on each section, a reference model under load case 2 (LC2) and load case 6 (LC6) was calculated. The models, the applied forces, and the life cycle results can be found in Table 16 and Table 17. The results of the finite element models were evaluated to compare the standard curves presented in chapter 6.4.1. In the further comparison, only the curves based on free corrosion in seawater are utilized, as the comparison to corrosion pits should be analyzed, for which free corrosion behavior has to be assumed.

LC2	Angle of load [rad]	Damage equivalent load [KN]	Nominal stress range [MPA]	Lifecycles air [E6]	Lifecycles seawater [E6]
Top	0.77	180.426	39.37	2587.3	343.9
Middle	0.58	181.697	43.24	1778.1	236.4
Bottom	0.14	190.045	57.32	575.5	76.5

Table 16: Load case 2 applied to the half-chain model and the resulting stresses.

LC2	Angle of load [rad]	Damage equivalent load [KN]	Nominal stress range [MPA]	Lifecycles air [E6]	Lifecycles seawater [E6]
Top	0.74	215.585	44.1	1634.8	217.3
Middle	0.56	219.149	56.2	621.0	82.6
Bottom	0.17	226.047	64.0	370.4	49.3

Table 17: Load case 6 applied to the half-chain model and the resulting stresses.

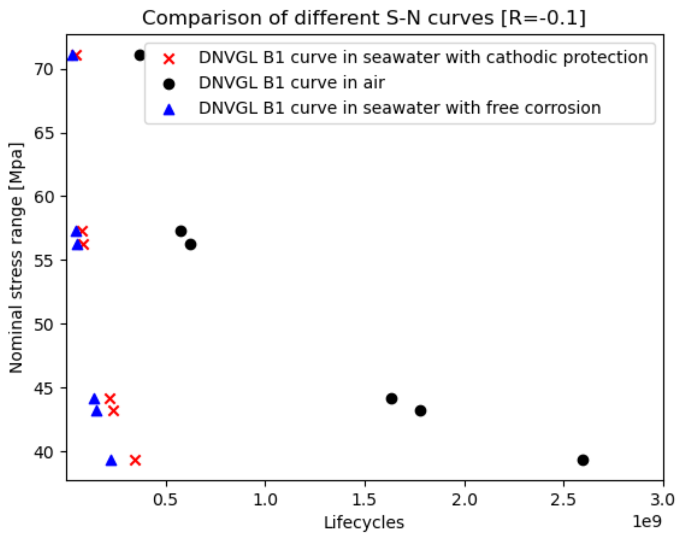

Figure 36: Comparison of the three given S-N curves based on results from LC2 and LC6.

7.2.3 FEM model with corrosion implementation

Different locations of corrosion pits were tested to find the placement with the highest resulting stresses. This model was then to be used for further analysis. The most likely locations were presented in chapter 6.4.1 based on *Mendoza et al.*. The results for these sections in regard to LC2 are given in the tables below.

Model	Angle of load [rad]	Damage equivalent load [KN]	Nominal stress range [MPA]	Lifecycles free corrosion [E6]	Corrosion decrease [mm]
Top	0.77	180.426	89.63	8.32	0.120
Middle	0.58	181.697	98.28	5.76	0.114
Bottom	0.14	190.045	111.78	3.44	0.105

Table 18: Life cycles under free corrosion with the influence of corrosion pits at the straight section.

Model	Angle of load [rad]	Damage equivalent load [KN]	Nominal stress range [MPA]	Lifecycles free corrosion [E6]	Corrosion decrease [mm]
Top	0.77	180.426	87.80	9.04	0.120
Middle	0.58	181.697	95.76	6.39	0.114
Bottom	0.14	190.045	107.91	3.96	0.105

Table 19: Life cycles under free corrosion with the influence of corrosion pits at the bend section.

Model	Angle of load [rad]	Damage equivalent load [KN]	Nominal stress range [MPA]	Lifecycles free corrosion [E6]	Corrosion decrease [mm]
Top	0.77	180.426	95.40	6.48	0.120
Middle	0.58	181.697	104.58	4.49	0.114
Bottom	0.14	190.045	117.09	2.86	0.105

Table 20: Life cycles under free corrosion with the influence of corrosion pits at the crown section.

To compare the results of the different locations of corrosion pits, a scatter plot including the different S-N results based on the free corrosion curve is presented in Figure 37. The corrosion rates that resulted in these stresses were corrosion rates after the first year of immersion. The presented results show a high reduction in fatigue life. As the corrosion pit is implemented in the bend where the coupling diameter is located, the force acts directly onto the corrosion pit, which could lead to high uncertainties. Implementing the pit in the crown section, as presented in Table 20 gives the highest lifecycle decrease. As this also is coherent with the highest fatigue crack rate being at the crown, this section was chosen for further analysis.

7.2.4 Comparison of FEM results pre-corrosion and post-corrosion initiation

To visualize the effect of corrosion on the number of lifecycles a mooring chain can endure at a given load, a comparison of the life cycles of the mooring chain before and after corrosion initiation under a chosen load case was examined. Eight load cases were chosen with a high probability of occurrence and are presented in Table 14. The curve considered for the S-N analysis is the free corrosion curve. A complete table of the load cases and resulting loads, lifecycles, and corrosion rates can be found in Appendix B.

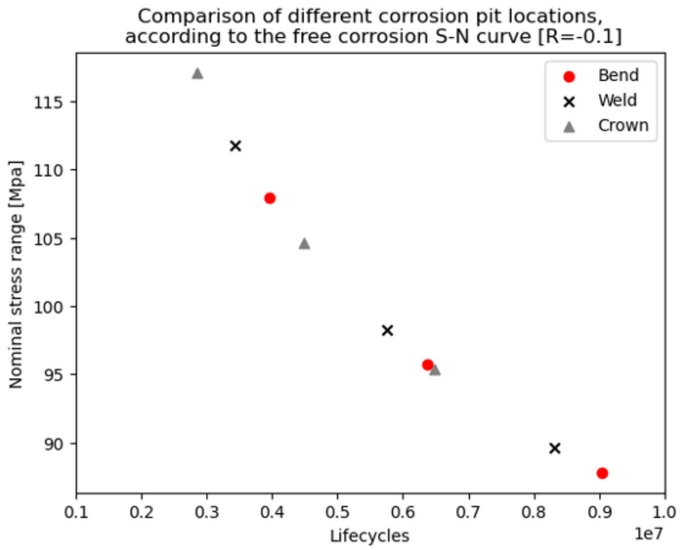

Figure 37: Comparison of lifecycle results based on different corrosion pit locations.

7.3 Comparison of FEM results of most probable load cases

The results of Table 14 presented load cases are shown in Figure 39. Here, the lifecycles of the nominal stress range in regard to pre-corrosion initiation are plotted against the post-corrosion initiation models.

It can be seen that the corrosion pits increase the stresses in the model, resulting in a lower number of life cycles compared to the model without corrosion pits. This leads to a decreased lifetime and possible weak points along the mooring line

The results of the most probable load cases were further analyzed to identify possible weak points along the mooring lines under load only and load in combination with corrosion. It became clear that the lowest lifecycle expectancy occurs with a high probability at the seabed. This is the case in both conditions of the mooring line, either with or without corrosion, despite the corrosion factor being the lowest in this region.

Section	Lifecycles [E6]	Corrosion decrease[mm]	Lifecycles free corrosion [E6]	Reduction of lifetime [%]
Top	225.32	0.120	6.48	97.12
Middle	154.85	0.114	4.49	97.10
Bottom	50.12	0.105	2.86	94.29

Table 21: Reduction of lifecycles through the implementation of corrosion at the crown in load case 2.

An interesting observation that can be made in Table 21 is that even though the weak point is regarding the lifecycles at the part close to the seabed, the reduction of lifetime is less. This is also represented in Figure The results presented in this chapter demonstrate the influence of corrosion and fatigue along the mooring line. The following chapter discusses the results in terms of their accuracy and applicability.

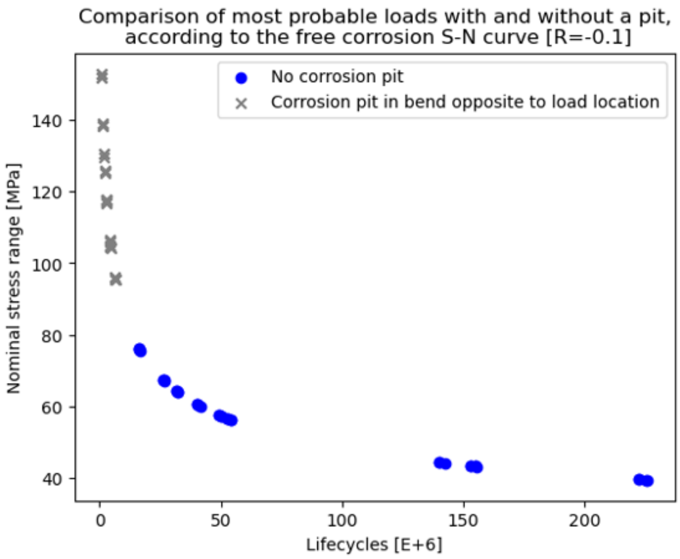

Figure 38: Comparison of results pre-corrosion and post-corrosion development after one year.

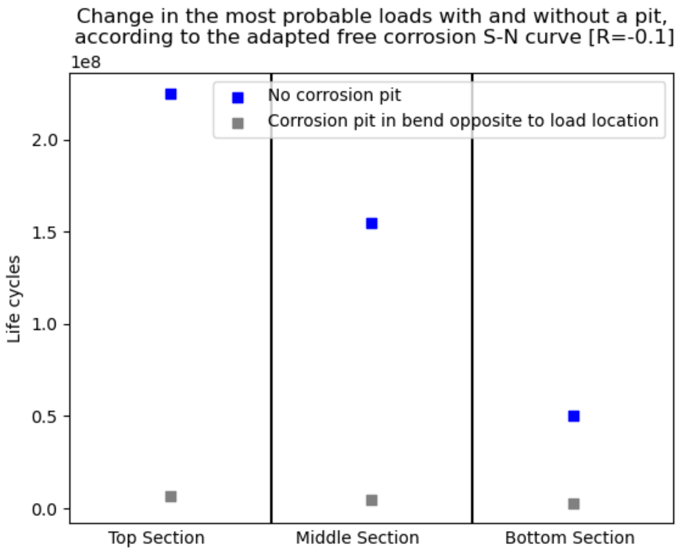

Figure 39: Comparison between results pre-corrosion and post-corrosion development after one year at the different chain segments.

8 Discussion

The research carried out throughout this thesis was intended to identify the combined effects of corrosion and fatigue along mooring lines. The results of the presented models showed that the proposed methodology leads to a determination of the combination of corrosion and fatigue effects along the mooring line. In the following paragraphs, this new approach is discussed.

8.1 Verification of the corrosion model

The developed corrosion model provides the possibility to calculate corrosion over depth and immersion time. The corrosion rate is relatively low compared to the standard value in the COREWIND project and other studies such as *Orlikowski et al.* [9].

For example, *Orlikowski et al.* [9] measured a corrosion rate of 0.4mm/year at the bottom of the Baltic Sea based on the corrosion of carbon plates. This indicates that the corrosion rate of $0.09 mm/year$ at the seafloor is relatively small. However, due to salinity and temperature, corrosion rates depend on varying effects in different seas. In addition, the steel used is different from the R4 mooring steel.

It also falls below the corrosion allowance described in the COREWIND project by *Vigara et al.* [1]. The corrosion allowance at the surface and seabed was given as 0.4mm/year and in the permanent submerged clay as 0.3mm/year.

In a publication by *Mendoza et al.* [11], mooring chains of different immersion years were analyzed for corrosion development and fatigue life. It has been shown that mooring lines made of R4 mooring material often remain below corrosion grade 1, representing corrosion with a pit size of less than 1 mm within the immersion rate of 10 years. This aligns with the newly developed model based on Nevshupa and Fickian. After the immersion time of 10 years, the corrosion pits in the extracted chains grow at a higher rate than the model.

This difference could be caused by neglecting the influence of micro biologically induced corrosion. Due to the lack of data at this location, microbial corrosion has been omitted but could lead to higher corrosion near the seabed and the water surface. As the OpenFast project mooring chain is only 15 meters below the surface, no splash zone or micro biologically induced corrosion had to be considered in the corrosion assumption for the chain. Therefore, only the corrosion rate close to the seabed is affected by neglecting the micro biologically induced corrosion.

8.2 Validation of OpenFast results

A model based on the IEA 15MW wind turbine has been implemented in the OpenFast software. This open-source model of the IEA 15MW has already been used in other projects, for example, in a study by *Hall et al.* [32]. Although this research tested the extreme loads of the FOWT IEA 15, pretension loads were also tested. As they used a pretension of 4 MN, it indicates that the magnitude of the force determined by the calculations is correct. The distribution of line loads is similar to Anchor 1, which takes the prevailing loads in the extreme calculations. The comparison of the research of *Hall et al.* to the OpenFast loads shows that the magnitude is similar.

Furthermore, the maximum load is less than 25% of the minimum breaking load, which is 17811.45 MN. This is an acceptable value for the maximum of the most probable loads.

Regarding the DELs, a comparison to the COREWIND project can be drawn itself. In the publication of *Cevasco et al.* [25] DELs were calculated as well for different sections of the mooring line. Two conclusions can be drawn from this matter. The first is that the range DEL is in an acceptable magnitude, as it is similar to the one determined by *Cevasco et al.* The second is that it is presented that the equivalent loads at the anchor section can indeed be higher than the one at the fairlead, and thus, the change in damage equivalent load along the mooring line is common.

8.3 Verification of the finite element model

As the FEM model, including the hot spot analysis, was carried out similarly to the model published by *Lassen et al.* [29], the basic model has already been verified by other authors. However, some adaptations have been made that need to be considered when discussing the model.

The diameter of the model is taken from the COREWIND project, and the dimensions were based on the standard diameter. The material properties are taken from the research of *Zarandi et al.* [19]. One option to verify the behavior of the FEM model is to look at the deformation of the chain and compare it with actual chain deformation. Presented in Figure 40, the deformation under minimum load is scaled up by 50, resulting in the colored deformed shape. The deformation through elongation at the straight part of the chain segment shows that the mooring chain behaves like a real chain under tension.

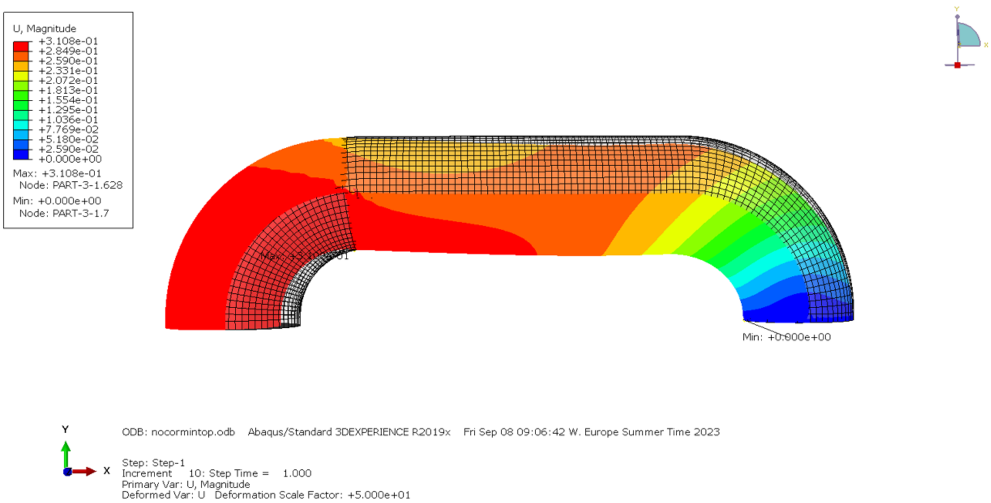

Figure 40: Deformation of the ABAQUS model utilizing an upscaling of the deformation by the factor 50.

The corrosion implementation is based on the vulnerabilities identified by *Mendoza et al.* [11]. As this implementation method is simple and uses only one corrosion pit, the influence of multiple corrosion pits on each other and the stresses were not included in the analysis. This implementation method has been used before, for example, in the publication of *Hove et al.* [33], but regarding stress corrosion cracking. To identify the fatigue life over the corrosion pit size, stress corrosion cracking implementation could also be a solution.

8.4 Validation of the fatigue analysis

The results of the models were analyzed regarding the S-N curves given in standard *DNGL-RP-CP203* [26] according to material B1. To check the correct implementation of the values of the S-N model, a comparison between the given and calculated results was executed as presented in Figure 41. Here, it can be seen that the curves almost overlap, indicating the correct application of the curve. Although this curve does not explicitly

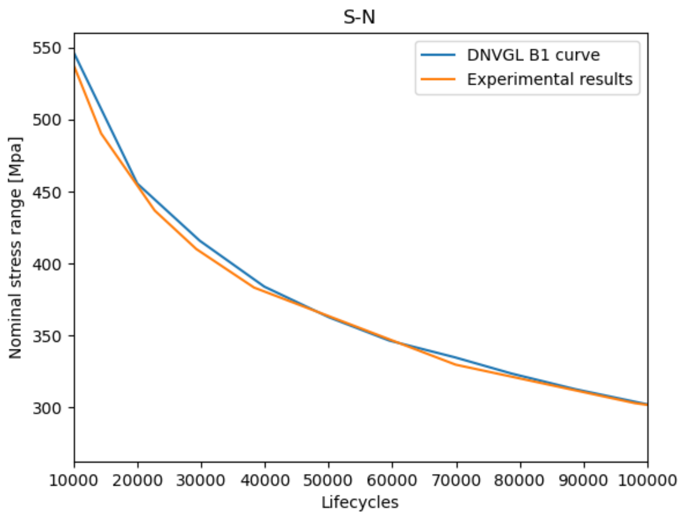

Figure 41: B1 S-N curve compared to the nominal stress range determined by ABAQUS implemented in the equation.

refer to R4, the steel properties are similar, and this curve has been used in previous research, for example, by *Mendoza et al.* [11], to determine fatigue life. Therefore, the use of this curve is recommended because it provides the possibility to compare the fatigue results to other research.

As shown in chapter 7, different load cases were carried out with respect to no corrosion and corrosion pits. It became clear that implementing corrosion pits into the model increases the stresses within the model by up to 200%.

This implementation led to reduced life cycles between 95-97%, as shown in Table 21. *Bayraktar et al.* cite[34] developed a comparison of an S-N curve between mooring chains and corrosion-induced mooring chains. Here, the life cycles between very high stresses were reduced, in some areas, by about 98%. As this reduction is nearly similar, it indicates that the results are according to experimental results, as *Bayraktar et al.* used steel probes under electrochemical influence and thus can resemble real-life conditions.

8.5 Weakpoint identification

Based on the results presented, it can be identified that weak points along the mooring chain could be identified based on fatigue and corrosion modeling. These weak points can lead to high uncertainties in the lifetime of the mooring chain because even though they only affect one section, the ability to produce renewable energy depends on it. Therefore, some possibilities to increase the safety factor of the weak points were identified. One of the more straightforward options would be to increase the diameter, giving a higher fatigue life and corrosion resistance. However, even this could cause problems in the design of the mooring chain, and if close to the seabed, a high number of segments would have to be built with a bigger diameter, leading to higher production costs. A further option would be implementing clump weight to hold down the catenary line in high offsets so that the line works as a taut system. This was suggested by *Hall et al.* [35]. Nevertheless, this weight could lead to higher wear at the mooring section, which is in contact with it.

9 Conclusion and future work

In this thesis, a representative finite element model of a mooring chain has been developed, incorporating a wide range of modeling factors to answer the research question: **"How can fatigue and corrosion be modeled to identify weak points along the mooring lines of floating offshore wind turbines?"**

The developed model was built based on the example FOWT near Gran Canaria presented in the COREWIND project. Utilizing this project, the research answered the following four subquestions.

How can corrosion be accurately modeled along the mooring line?

A depth and immersion time-dependent corrosion model was determined based on a short-term corrosion initiation model and a long-term immersion model. The corrosion model was adapted to the site using extracted temperature and oxygen data based on water depth. Using this data, a corrosion model was developed to determine corrosion rates at any point in the water column and the immersion life of chains made of R4 mooring steel.

How can fatigue be accurately modeled along the mooring line?

A model of tension in mooring lines was determined using the OpenFast software. This software implemented the COREWIND wind turbine and environmental data, calculating the tensions along the mooring. These load histories of the tensions were the translated into damage equivalent loads. In a finite element model, these damage equivalent model was then used to implement the mooring line tensions on the mooring chain segments along the mooring line. A finite element model of a half-mooring chain segment was built based on the mooring chain of the OpenFast model. The model itself was fine-tuned using a mesh convergence and coupling study. The effects of hydro static pressure and out-of-plane bending were included in the model for the pure tensile fatigue life determination. Based on the OpenFast calculations, the maximum stresses through the loads could be found in the chain segment, and S-N curves were used to calculate the fatigue life based on these stresses.

How do fatigue and corrosion interact?

A stress-corrosion model was built using both of the above-validated methods. The effect of corrosion on fatigue life was tested. It was found that even though corrosion can be low, it can affect the fatigue life. Using this model, it was possible to determine that there were weak points along the mooring line, mainly when corrosion and fatigue occurred in combination.

How can the weak points be improved?

The weak points were identified based on fatigue life established by the loads' intensity and the corrosion rate. The corrosion rate is highest in the higher areas of the water column. Under high loads, these are also the areas of the mooring chain where the highest stresses occur.

For future research, more aspects could be implemented to increase the model's accuracy. In the corrosion model, the bacterial influence near the seabed could be included as it also increases the corrosion rate in the lower part of the chain. Regarding load determination, the influence of the neglected TFI spring could be applied to see the effect of reducing the peak loads on the probability. The effect of residual stresses could be implemented within the finite element model. This would allow the implementation of the proof load and structural residual stresses such as the weld. In addition, seabed friction can be included in the model for the lower part of the mooring chain.

It can be concluded that with the presented methodology, it was possible to create a new method for determining critical regions within the mooring chains of floating offshore wind turbines. By following the steps described in the methodology, it can be reproduced based on other floating offshore wind turbine projects. Furthermore, it can be used in the design of floating offshore wind turbine mooring systems to identify and prevent weak points and thus reduce the risk of mooring line failure in the future.

References

[1] Fernando Vigara, Lara Cerdán, and Rubén Durán. D1.2 Design Basis. Technical report, 2020.

[2] Rebecca Williams, Feng Zhao, and Joyce Lee. Global Offshore Wind Report 2022. Technical report, Global Wind Energy Council, Brussels, 6 2022.

[3] Josep Lloret, Antonio Turiel, Jordi Solé, Elisa Berdalet, Ana Sabatés, Alberto Olivares, Josep Maria Gili, Josep Vila-Subirós, and Rafael Sardá. Unravelling the ecological impacts of large-scale offshore wind farms in the Mediterranean Sea. *Science of the Total Environment*, 824, 6 2022.

[4] Charalampos Baniotopoulos. Advances in Floating Wind Energy Converters. *Energies 2022, Vol. 15, Page 5658*, 15(15):5658, 8 2022.

[5] E. Fontaine, A. Kilner, C. Carra, D. Washington, K. T. Ma, A. Phadke, D. Laskowski, and G. Kusinski. Industry Survey of Past Failures, Pre-emptive Replacements and Reported Degradations for Mooring Systems of Floating Production Units. *Proceedings of the Annual Offshore Technology Conference*, 3:2038–2051, 5 2014.

[6] Kai Tung Ma, Yong Luo, Thomas Kwan, and Yongyan Wu. Mooring system engineering for offshore structures. *Mooring System Engineering for Offshore Structures*, pages 1–350, 1 2019.

[7] R Nevshupa, I Martinez, S Ramos, and A Arredondo. The effect of environmental variables on early corrosion of high-strength low-alloy mooring steel immersed in seawater. 2018.

[8] Øystein Gabrielsen, Turid Liengen, and Solfrid Molid. Microbiologically Influenced Corrosion on seabed chain in the North Sea. *Proceedings of the International Conference on Offshore Mechanics and Arctic Engineering - OMAE*, 3, 2018.

[9] Juliusz Orlikowski, Michał Szociński, Krzysztof Żakowski, Piotr Igliński, Kinga Domańska, and Kazimierz Darowicki. Actual field corrosion rate of offshore structures in the Baltic Sea along depth profile from water surface to sea bed. *Ocean Engineering*, 265:112545, 12 2022.

[10] Junfeng Du, Hongchao Wang, Shuqing Wang, Xiancang Song, Junrong Wang, and Anteng Chang. Fatigue damage assessment of mooring lines under the effect of wave climate change and marine corrosion. *Ocean Engineering*, 206:107303, 6 2020.

[11] Jorge Mendoza, Per J. Haagensen, and Jochen Köhler. Analysis of fatigue test data of retrieved mooring chain links subject to pitting corrosion. *Marine Structures*, 81:103119, 1 2022.

[12] Wentao He, Shihui Cao, Zhiqiang Hu, De Xie, Zhengyi Zhang, and Changzi Wang. Numerical evaluation on fatigue crack growth and life predictions of an FPSO mooring system. *Ocean Engineering*, 265:112501, 12 2022.

[13] Erling N Lone, Thomas Sauder, Kjell Larsen, Equinor Asa, and Bernt J Leira. Fatigue assessment of mooring chain considering the effects of mean load and corrosion. 2021.

[14] Ángela Angulo, Graham Edwards, Slim Soua, and Tat-Hean Gan. Mooring Integrity Management: Novel Approaches Towards In Situ Monitoring. *Structural Health Monitoring - Measurement Methods and Practical Applications*, 6 2017.

[15] J Jonkman. Definition of the Floating System for Phase IV of OC3. 2010.

[16] Gustavo Sánchez, Alberto Llana, and Gonzalo Gonzalez. D1.1 Oceanographic and meteorological conditions for the design Disclaimer Document information. 2015.

[17] Wei Shi, Lixian Zhang, Madjid Karimirad, Constantine Michailides, Zhiyu Jiang, and Xin Li. Combined effects of aerodynamic and second-order hydrodynamic loads for floating wind turbines at different water depths. *Applied Ocean Research*, 130, 1 2023.

[18] Jennifer Rinker and Witold Skrzypinski. COst REduction and increase performance of floating WIND technology (COREWIND) H2020-LC-SC3-2018-RES-TwoStages / Grant Agreement 815083 D1.1 Definition of the 15 MW Reference Wind Turbine. Technical report, 2020.

[19] Ershad P. Zarandi and Bjørn H. Skallerud. Experimental and numerical study of mooring chain residual stresses and implications for fatigue life. *International Journal of Fatigue*, 135, 6 2020.

[20] Lucas Méchinaud, Florian Castillo, Mohammad Youssef, Mahfouz Ustutt, Leonard Willeke, and Henrik Bredmose. corewind D2.3 Exploration of innovations and breakthroughs of station keeping systems for FOWT 2 Document information Deliverable number D2.3 Deliverable name Exploration of innovations and breakthroughs of station keeping systems for FOWT Work Package and Task WP2-Design and optimization of station keeping systems Task 2.3-Exploration of innovations and breakthroughs of station keeping systems for FOWT. 2022.

[21] Requirements Concerning Materials and Welding, W22 Offshore Mooring Chain, 2011.

[22] Erling N. Lone, Thomas Sauder, Kjell Larsen, and Bernt J. Leira. Probabilistic fatigue model for design and life extension of mooring chains, including mean load and corrosion effects. *Ocean Engineering*, 245, 2 2022.

[23] Fabian Wendt, Amy Robertson, Jason Jonkman, and Morten T Andersen. Verification and Validation of the New Dynamic Mooring Modules Available in FAST v8: Preprint. 2016.

[24] Bonnie Jonkman and Jason Jonkman. FAST v8.16.00a-bjj. 2016.

[25] Debora Cevasco, Ramboll Jannis, Tautz-Weinert Ramboll, Marie-Antoinette Schwarzkopf, Friedemann Borisade, Ramboll Moritz, Häckell Ramboll, Qi Pan, and Mohammad Youssef Mahfouz. COREWIND D4.2 Floating Wind O&M Strategies Assessment 2 Document information Deliverable number D4.3 Deliverable name Condition Monitoring Strategies for Floating Wind O&M Authors Name Organisation Version control RAMBOLL Final version for submission.

[26] DNV-RP-C203 Fatigue design of offshore steel structures - DNV. Technical report.

[27] Tim P. Boyer, Hernan E. Garcia, Ricardo A. Locarnini, and Melissa M.. Zweng. World Ocean Atlas 2018., 2018.

[28] Robert E. Melchers. Predicting long-term corrosion of metal alloys in physical infrastructure. *npj Materials Degradation 2019 3:1*, 3(1):1–7, 1 2019.

[29] Tom Lassen, Eirik Storvoll, and Arild Bech. Fatigue life prediction of mooring chains subjected to tension and out of plane bending. 2009.

[30] Ershad P. Zarandi and Bjørn H. Skallerud. Cyclic behavior and strain energy-based fatigue damage analysis of mooring chains high strength steel. *Marine Structures*, 70, 3 2020.

[31] Wendell S. Brown. Physical properties of seawater. *Springer Handbook of Ocean Engineering*, pages 101–109, 1 2016.

[32] Matthew Hall, Ericka Lozon, Stein Housner, al , Qi Pan, Mohammad Youssef Mahfouz, and Frank Lemmer. To cite this article: Qi Pan et al 2021. *Journal of Physics: Conference Series*, page 12030, 2018.

[33] Martin Hove and Jochen Köhler. Growth of Fatigue Cracks in Mooring Line Chains. *95*, 2016.

[34] Emin Bayraktar, Rubén Mora, I. M. Garcia, and Claude Bathias. Heat treatment, surface roughness and corrosion effects on the damage mechanism of mechanical components in the very high cycle fatigue regime. *International Journal of Fatigue*, 31(10):1532–1540, 10 2009.

[35] Matthew Hall and Andrew Goupee. Validation of a lumped-mass mooring line model with DeepCwind semisubmersible model test data. *Ocean Engineering*, 104:590–603, 6 2015.

A Appendix A

Faculty Mechanical, Maritime and Materials Engineering

MSc Offshore and Dredging Engineering

Literature Review

A Finite Element Analysis Investigation of Fatigue and Corrosion of Floating Offshore Wind Turbine Mooring Lines

Author:

Theresa Beer

5569435

Supervisor:

PhD Andrea Coraddu

PhD Olena Karpenko

28.02.2022

1 Abstract

Floating wind turbines are becoming increasingly important in the renewable energy sector, especially in countries where the water depth is too deep for conventional monopile structures. Mooring lines are required to keep these floating wind turbines in place, both in good weather conditions and during storms that bring strong winds and high waves. It is important to ensure that these mooring lines are in good condition throughout their lifetime. Degradation of the line, such as breaks or deformation, can lead to reduced functionality or, in the worst case, complete failure of the system. Therefore, they need to be monitored and maintained over their lifetime. However, monitoring equipment can often be expensive and maintenance time-consuming. Another way to assess the degradation of mooring lines is to create a data-augmented numerical model. This allows the possible effects of sea state and environmental forces on the mooring line to be simulated to determine its lifetime and degradation. The state-of-the-art numerical simulation techniques of these models can now provide important information on the effects of different load cases on the mooring lines through the input of different forces, weather conditions and also material wear. The following literature review will serve as the basis for a Master's thesis that presents the current state-of-the-art in fatigue damage assessment techniques, with a particular interest in the implementation of corrosion. It was found that although corrosion and fatigue have been modelled together, the influence of corrosion has often been neglected or considered a conservative factor. The superposition of corrosion and stress was found to cause weaknesses in combination with other factors. Based on these findings, research questions were developed for the subsequent Master's thesis.

Contents

Nomenclature

α	Crack Depth
ΔK	Amplitude of stress intensity factor
σ	Stress acting on mooring chain
C, m	Paris constants
C_B	dissolved oxygen rate in bulk waters
C_t	dissolved oxygen concentration
D	Chain Diameter
$g_1(\sigma_m)$	Function of the mean stress
$g_1(c)$	Function of corrosion grade
K	Intercept parameter
K_{th}	fatigue threshold
m	Slope of S$_N curve$
N_f	Number of future years
N_p	Number of prior years
n_{si}	Number of tension cycles
N_s	Number to failure
P_i	Occurrence probability
T	Temperature
t	Simulation duration
U	Stress range
v	Velocity
Y	Stress intensity correction factor
Z_k	Fatigue load for the k-th year
A	Intercept parameter
b0 - b2	Uncertainties of the capacity model

Acronyms

FOWT Floating Offshore Wind Turbine. 2, 11, 23, 25

PRQ Preliminary research Questions. 3, 4

RAO Response Amplitude Operator. 11

RQ Reasearch Questions. 24

SCC stress corrosion cracking. 10, 18, 23, 24

2 Introduction

Due to changes in energy resources in recent years, more and more wind turbines are being built. By the end of 2021, the total installed offshore wind capacity in Europe will reach 21.1 gigawatts [1]. As more and more wind turbines are installed offshore, less area is available in the shallower parts of the oceans. In addition, countries where the continental shelf drops off abruptly close to the coast also want to install wind turbines [2]. This has led to the development of floating offshore wind turbines , which allow wind energy to be generated in deeper waters. Unlike conventional offshore wind turbines, these special turbines are not installed on a monopile on the seabed but on floating pontoons held in place by mooring lines. The first floating offshore wind farm was installed in 2017, and since then, the installed capacity of floating offshore wind in Europe has reached 73.33 MW [3]. With new innovations come new problems, in fact, as reported by *Fontaine et al.* [4], half of the turbine failures were caused by mooring line failure, of which half were caused by **corrosion** and **fatigue**. These figures have also been found in the oil and gas industry, which has been using mooring lines to hold floating production vessels in place since 1977 [5]. As this problem does not only occur in new industries but has been a problem for years, it has led to a loss of investment for decades [4]. In order to solve this problem, studies have been carried out and further mooring line models have been developed. In the following document, a literature review is presented to investigate the research that has already been executed. The third chapter provides the background and motivation for the literature review. The fourth chapter presents the literature review. Firstly, the approach to the quality requirements of the papers used in this literature review is explained and secondly, the literature review is carried out. This is followed by an explanation of the fatigue assessment methods and then the combination of corrosion and fatigue modelling solutions. Further weak points along the mooring line are investigated. Based on chapter five, a reflection is made in which the preliminary research questions are answered and the final research questions that will be used in the Master's thesis are determined. Finally, a preliminary methodology to answer the research questions is presented.

3 Background and Motivation

Since the start of the offshore oil and gas industry, many important developments have made it the major industry it is today. One notable step was the first use of floating drilling vessels in 1955, which ushered in the era of floating oil exploration. This was quickly followed by fixed installations in 1977. Today, various types of floating oil and gas systems can operate in water depths of up to 3000 meters [5]. As these floating systems operate mainly in deep waters, they have become examples for the offshore wind industry, where the transition to deeper waters came in 2009 with the deployment of the first floating offshore wind turbine (FOWT) off the coast of Norway [5].

Offshore wind energy has the advantage of larger available areas and no wind coverage; more energy can be produced by using a larger wind park size with larger turbines [6]. A further shift of wind energy towards offshore has the advantage of reducing political restrictions [7]. As has been shown in several countries, onshore wind faces strong opposition from the public and tourism associations [8]. Offshore wind, which is ground based, faces its biggest hurdle with water depth, one point being that the cost of onshore monopile structures increases with water depth, the move towards floating offshore wind is recommended [9]. Since 2009, many more FOWT have been built, with a total capacity of 121.4 MW to date, rising to 6900 MW by 2030 [1]. This new technology opens up more areas for renewable energy production, especially for countries with narrow continental shelves, which can use the wind energy produced to drive forward the energy transition [2]. This can help reduce the use of fossil fuels and help countries become independent of oil, gas and coal [10]. The anchoring of the mooring lines replaces the hammering of the monopile, which protects animals from high noise emissions and makes decommissioning easier at the end of its service life [11, 12]. While floating wind turbines offer new energy resources with the above-mentioned benefits, the new types of substructures for wind turbines also pose risks [5]. As described in [13], failure of the mooring system is the second-highest risk of failure, after the wind turbine itself. This has also been reported in the oil and gas industry, where up to 50% of failure events on floating platforms are caused by mooring system failure. Of these failures, up to 65% were caused by corrosion and fatigue, as shown in Figure 1 [14]. The potential failure of a mooring line can therefore result in environmental risk, loss of capital and danger to any maintenance personnel involved. The problem with high turbine failure rates is not only the loss of turbine production itself, which would result in a loss of capital but also damage to the turbine structure itself [16]. It has been found by *Zhang et al.* [16] that breakage of mooring lines under certain conditions can lead to changes in structural responses that can damage the turbine itself in the long run [16]. Further failure of a mooring line can increase the stresses in the remaining lines, which, if the line is repaired, can cause fatigue problems in the future [16]. As it is often difficult to know when a mooring failure has occurred, the platform can drift up to 700 metres, which can pose a risk to other wind turbines in the same wind farm, resulting in further loss of production [17, 13]. Furthermore, broken mooring lines can cause damage to the seabed, potentially harming the environment. All of these problems can lead to high capital loss if multiple failures occur, as offshore repairs are costly and time-consuming [13]. The installation of sensors and annual inspections could be used to prevent mooring line failure. However, these are often costly and time-consuming as mooring lines can be several hundred metres long. They can also include noise, which can interfere with the interpretation of results [18]. Other, FOWTs are located far offshore, so maintenance

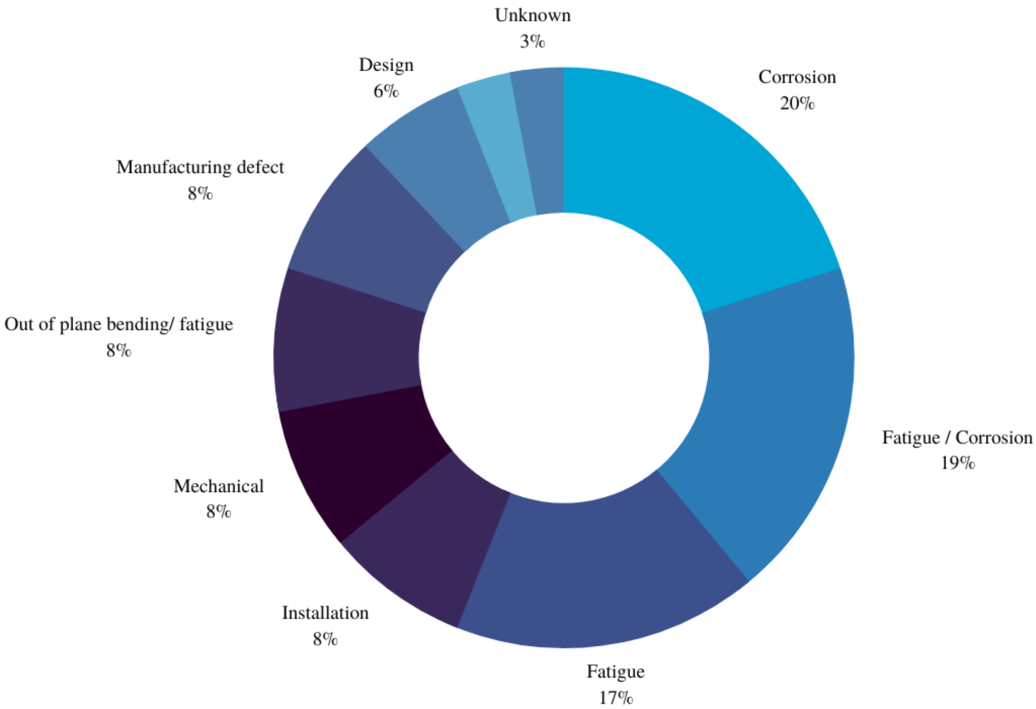

Figure 1: Causes of mooring line failure presented in terms of probability of occurrence[15, 14].

cannot be carried out as often as desired [19]. Therefore, the life prediction of mooring systems must be accurately calculated in the design phase of the FOWT and the dimensions of the mooring lines must be adapted to the environmental conditions. Another important aspect in predicting mooring line life is climate change. As described by *Du et al.* [20], several studies have shown that due to climate change, the 50-year wave height and the average wave height and wind speed are increasing. These research results show that future anchor line designs will need to take such changes into account as they may lead to increased failure events. In particular, these influences on the risk of corrosion and fatigue are important, as they account for 50% of the causes of failure. Another interesting aspect of the assessment presented by [4] shows different sections of the mooring line where it can fail. It is important to study the corrosion and fatigue influence of the degradation of mooring lines, as they are used not only in FOWT, but also in FPSOs, ships and other renewable energies. As mentioned in [21], accurate models of corrosion need to be developed to improve failure rates in the future. This is also of interest to the scientific community.

In the following literature review, the current state of research on mooring lines will be addressed with the following Preliminary Research Questions (PRQ):

PRQ (1): How do corrosion and fatigue affect the estimated service life of a mooring line?
PRQ (2): How are fatigue and corrosion considered in the design of mooring lines?
PRQ (3): How do corrosion and fatigue affect each other?

PRQ (4): Are there areas of increased deterioration along the mooring line?

To answer these questions, the effects of fatigue and corrosion on the mooring line are considered. In particular the methods and equations used to represent corrosion and fatigue in mooring line research, but also general seawater corrosion in relation to steel are investigated. The synergy between corrosion and fatigue and its influence on the life of the mooring lines is also considered. Further research into weak points along mooring lines and the possible effects of corrosion and fatigue on them is presented.

4 Literature review

In the following, a literature review is executed to determine how far research has progressed on corrosion, fatigue and the combined effect of both on mooring line degradation. First, the rationale used to determine relevant and scientific papers is described in 4.1, then the literature review is executed where the current research regarding corrosion, chapter 4.2, fatigue, chapter 4.3, their combination, chapter 4.4 and weakpoints, chapter 4.5 along the mooring line are presented.

4.1 Literature review approach

In the following literature review, the sources used were considered only if of a certain quality, according to the following KPIs:

- H-index
- quartile
- impact factor
- publication date

The decision process is carried out using quality criteria to classify the quality of the papers. The main criteria used in the following work are the quartile and the H-index. The quartile criterion is divided into classes from Q1 to Q4. Q1 defines the highest quality of a journal, and Q4 is the lowest. Only papers in journals with a Q1 or Q2 rating are used in the following literature review. If papers from journals with a Q2 rating are used, the impact factor or H-index have to be equivalent to a Q1 journal rank. The H-index is a criterion that describes how often a paper has been cited in other published papers. It can also be used to indicate whether a paper is relevant or not. Another important aspect of including relevant papers in research is that they are up-to-date and have been published in recent years. In Figure 2, the decision process for determining whether a journal is of acceptable quality is given.

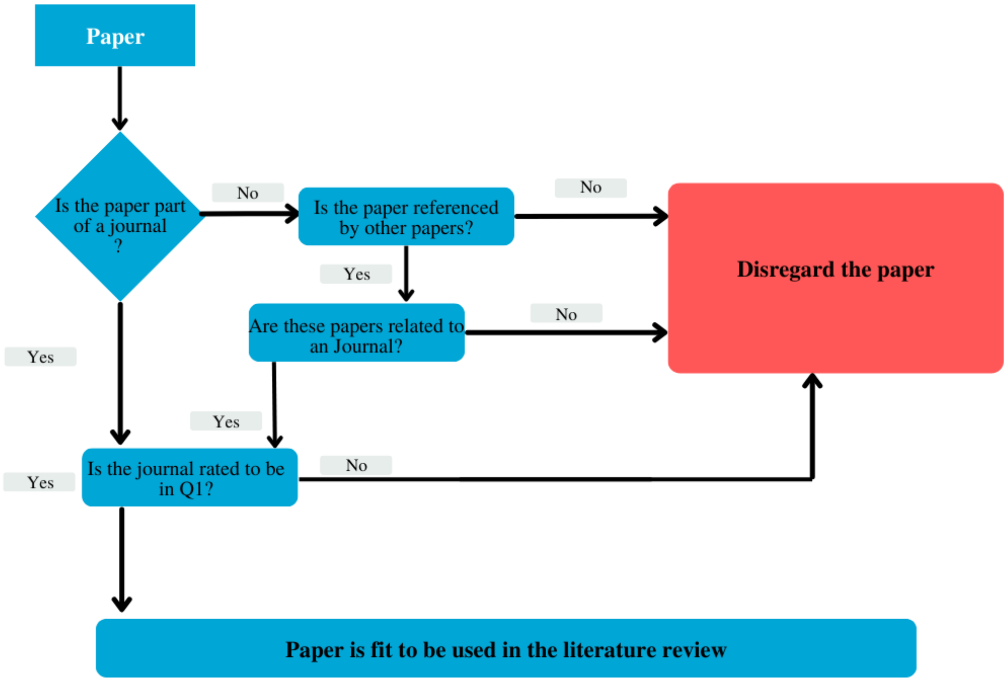

Figure 2: Flowchart describing the decision process for selecting eligible papers.

Figure 3 shows the years in which the papers were published. This graph shows that the research presented in the following literature review is up to date.

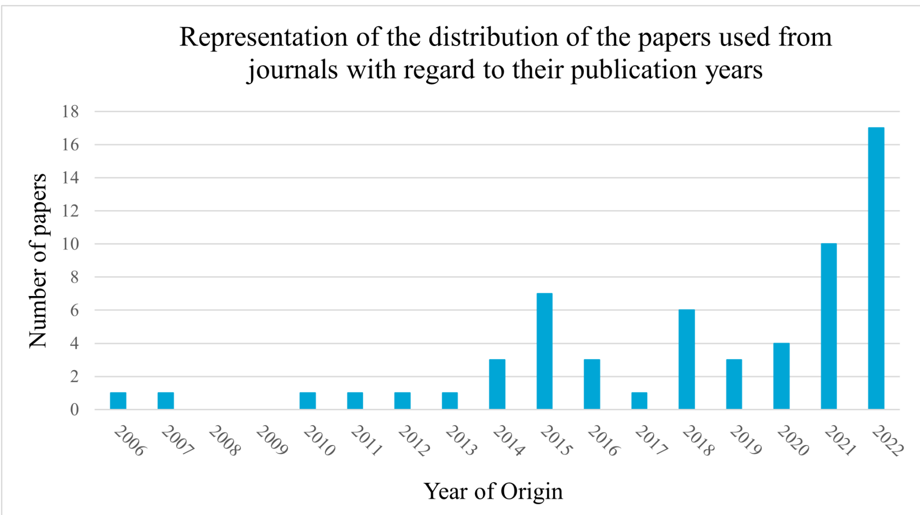

Figure 3: Publication years of research papers used in the literature research.

Table 1, summarises the considered journals, their impact factor and H-index and further the amount of papers extracted from them.

Journal	**Impact Factor**	**H-index**	**Papers**
Ocean Engineering	4.73	109	28
Marine structures	4.52	71	8
Applied Ocean Research	4.12	74	4
Renewable Energy	8.634	210	3
Renewable & Sustainable Energy Reviews	14.98	337	2
Corrosion Science	7.43	219	2
Energies	3.25	111	2
Science of The Total Environment	7.963	275	1
Materials Science & Engineering A: Structural Materials	5.23	252	1
Journal of the Mechanics & Physics of Solids	5.582	181	1
IEEE Access	3.37	158	1
Environmental Research Letters	6.41	142	1
Materials Characterization	4.36	104	1
Wind Energy	3.71	98	1
Energy research and Social Science	6.83	76	1
Theoretical & Applied Fracture Mechanics	4.24	65	1
Journal of Marine Science & Technology	2.38	50	1
Ships & Offshore Structures	1.97	32	1
Journal of Marine Science & Engineering	2.57	29	1
Total number of papers extracted from Journals			**61**

Table 1: Summary of the journals from which papers were extracted

Important research can be based on conference papers, which do not have the extensive peer review process of high-quality journals. In order to use conclusions that are important insights, the author decided, based on the quality and content of the conference paper, whether it would have been worth including it or not.

4.2 Mooring line corrosion

There are multiple influences on the fatigue life of a mooring chain, such as wear, tear and corrosion. In the offshore industry corrosion is one of the main factors for damage and failure of single parts, structures and elements. This often leads to downtime, loss of money, and, in the worst case, human injury or death. To determine the longevity of a mooring line during the design phase, it is necessary to work with a model and implement corrosion accordingly.

To estimate the corrosion development within the ocean there have been multiple studies. As offshore structures are often made of steel, the main factors that cause corrosion are water, salts, sun, oxygen, bacteria and surface stress.

As described by *Nevshupa et al.* [22] corrosion intensifies with the increase of temperature and dissolved oxygen in the seawater. Oxygen is dependent on temperature and the oxygen contingent in the water decreases with increasing temperature. Further salinity is an important aspect. It was found that the corrosion rate increases when the salinity in especially high or low, which is connected to the dependence of oxygen and carbon towards salinity.

A result of this study was the developed graph in Figure 4, which presents the corrosion rate dependent on the oxygen and temperature for an R4 mooring steel in synthetic sea water.

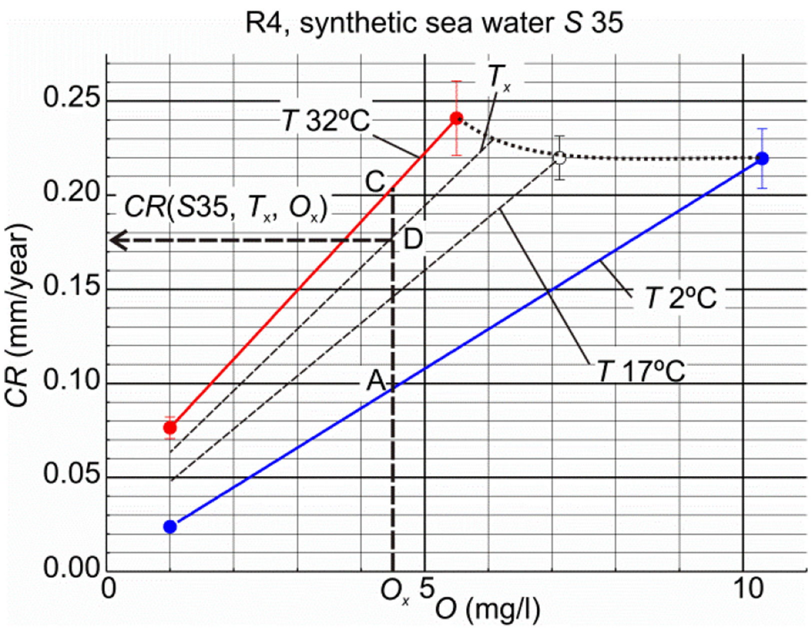

Figure 4: Corrosion rate per year plotted against the oxygen solution in water including influences of temperature and salinity[22].

Melchers et al. [23] also developed a equation to describe the corrosion rate dependent on temperature, presented in equation 1.

$$r_o = 0.056e^{0,065T}\frac{C_i}{C_B}(1+4,6V) \tag{1}$$

with C_t being the dissolved oxygen concentration, C_B the dissolved oxygen rate in bulk waters and T and v the temperature (range of $5C$ to $30C$) and the Velocity (range of 0 to $0.45\frac{m}{s}$) respectively. As described by *Olikowski et al.* [24] these factors are distributed differently in the water column, causing the water column to be divided in different zones. The highest zone is called the splash zone, where contact with the water is caused by different wave heights. Here, offshore structures are often protected by coatings, as the alternation of contact between water and oxygen causes a particularly high corrosion rate. The zone below is called the tidal zone. This zone is also subject to varying water heights, but due to high and low tides, and the structure is still protected by a coating.

From this zone to slightly above the sea bed is the immersion zone. The structure is permanently surrounded by water and the corrosion rate is very low due to the lower oxygen concentration. At the bottom of the sea is the sea bed zone, where the oxygen level remains low, but bacteria are added which accelerate the corrosion. The same happens in the marine sediment zone below.

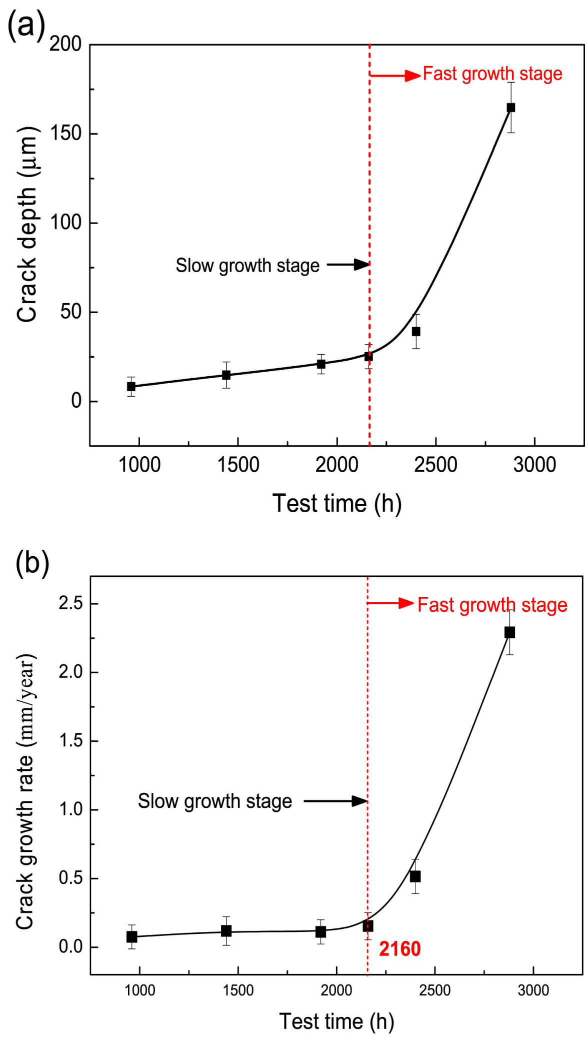

Figure 5: Crack deepening and corrosion development plotted against immersion time [25].

As seen above the corrosion rate can vary with the depth of the immersed mooring chain. As described by *Melchers et al.* [23] the corrosion rate can also vary over the time that the corrosion is immersed. This was supported by the findings of *Hao et al.* [25] for the splash or tidal zone where a constant change between wet and dry material occurs. Looking at the corrosion in specific development on the single mooring chain segments, interesting development could be detected. When corrosion is initiated on the mooring line, it will begin in the form of pitting corrosion an develop towards uniform corrosion.

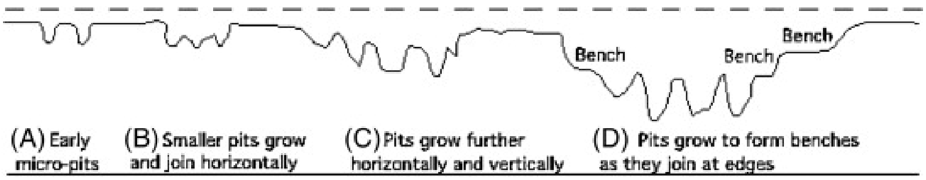

Figure 6: Depiction of the development from corrosion initiation to uniform corrosion on the mooring chain surface [26].

This process can also be seen in Figure 6. Since mooring lines are made of high strength steel, the pitting is not deep, as it is usually the case with stainless steel, but rather shallow and large [27]. After initiation, the pits start to develop in the horizontal plane. This leads to uniform corrosion which leads to an impact on the entire surface, also shown in [28].

Zhang et al. [29] found that stress at these corrosion pits causes micro cracks. This process is called the stress corrosion cracking (SCC) and is caused by strain in the mooring chain. In the research of *Olikowski et al.* [24] it was found that the corrosion rate at the sea surface in the Baltic sea can be higher than 0.8 mm/year in the Baltic sea and higher than 0.4mm/year at the sea floor. In other researches corrosion in mooring line is modeled as an approximation of 0.6 mm a year [30, 31]. A possibility to predict corrosion is usage of neural networks. As developed by *Kamrunnahar et al.* [32] the corrosion was predicted by using multiple parameters of corrosion, as corrosion rate based on polarization and corrosion data collected from experimental studies. Besides reducing the diameter of the mooring chain corrosion can also have an impact on fatigue cracks [33]. In the following chapters fatigue and the interaction of corrosion and fatigue are investigated.

4.3 Fatigue in mooring chains

Fatigue of offshore mooring lines can be determined in a number of ways. The process of determining mooring line fatigue consists of calculating the loads on the mooring lines and the resulting stresses in the chain segments. These can then be converted into fatigue cycles using accumulation techniques and counting methods to compare with experimental data and determine fatigue life. There are numerical, probabilistic and neural network approaches to determining future tensions, stresses and fatigue in mooring lines. The methods and steps are described in more detail below [34].

4.3.1 Assessment of tensions and stresses in mooring lines

Floating structures are subject to varying cyclic loads from waves, wind and currents, resulting in motion responses and subsequent mooring line tensions or stresses [35]. These mooring line stresses can be measured directly on the mooring lines themselves to help predict future extremes, or as presented by *Sauder et al.* [36] to build digital twins. As accurate measurement of data is often costly and time-consuming, a more reliable and commonly used option is to use hind cast data from a shorter time period and apply it to the lifetime of an offshore installation. In order to calculate the stresses or strains caused by these loads, environmental data such as wave height, scatter, wind direction, wind speed, etc. must first be determined. For this assessment, the first step is to select the location of the platform to be analysed. To determine site specific environmental data measurements of wind, waves and currents can be used and correlated with location, tides and seasons. This specific environmental data can then be analysed and utilised to determine the loads that can be used in fatigue analysis, as seen in Figure 7. The calculation of the resulting mooring forces using different models is discussed in more detail below.

Wave loads can be estimated using the Morrison equation and the Jonswap spectrum. Firstly, the Morrison equation is used to estimate the force of the waves on the FOWT using the drag force and the inertia force. The Jonswap spectrum is then used to determine a wave spectrum to simulate the waves. Wind loads acting on the FOWT are also considered by *Gao et al.* [38] and included as a drag force as an average over one hour. Current forces can be assumed to be steady. Wave frequency effects can be estimated from the wave spectrum and the FOWT response amplitude operators (RAO's).

To determine the corresponding FOWT motion forces from wind, wave and platform data at mooring lines, the time or frequency domain can be used. Both wave frequency and low frequency components can be estimated from wave spectrum and then combined with the response of the FOWT or quadratic transfer function for surge, sway and heave respectively [39]. These can then be used as input for time, frequency or spectral domain analysis. Because the time domain provides a more accurate method by taking into account so-called random wave characteristics and non-linear coupling between structural response and environmental influence, it is commonly used [40]. On the contrary, according to *Xu et al.* [41], the spectral method is more adequate because it is able to represent structural fatigue changes.

To determine the line stress, quasi-static or dynamic models can be used. According to *Hall et al.* [42], when comparing quasi-static approaches with dynamic approaches, it was found that it is useful to use quasi-static approaches for slack-mounted structures or for preliminary studies where accuracy is not the primary concern

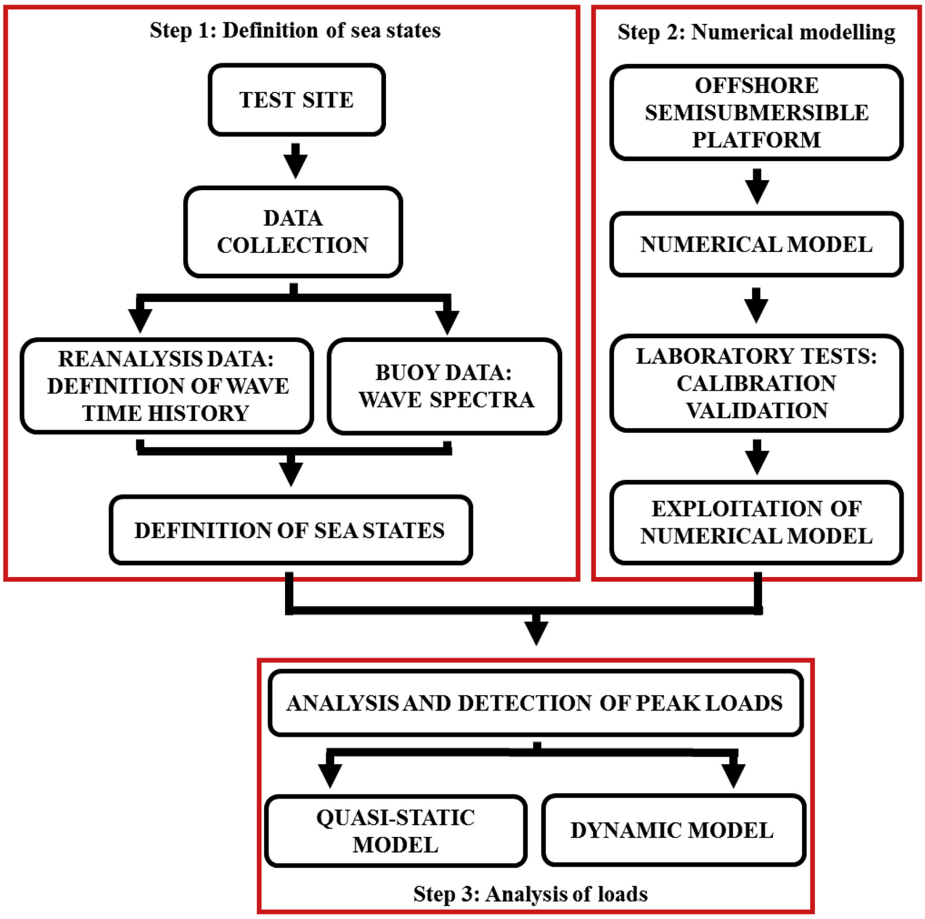

Figure 7: The process of determining mooring line tensions from environmental data and platform responses [37].

, as the numerical resolution is quite low compared to dynamic analysis [39]. For quasi-static approaches, the stress equation can be found in [43]. The main characteristic of the quasi static model is that it neglects dynamic effects such as damping, additional mass and inertia [44]. This leads to the inability to compute properly non-linear problems such as the impact of rogue waves [45]. In the general tension equation given in *El Beshbichi et al.* [19], the stress is generated by the time-invariant parts of the pre-stress and the mean line stress and the random processes by the wave frequency and the low frequency responses of the structure. Another approach could be the usage of dynamic methods, such as finite element methods (FEM) or lumped mass models [46]. For dynamic analysis using the finite element method, software such as ABAQUS or ANSYS can be used. Often only the interaction part of mooring chains is modelled, as presented in Figure 8. By inputting the previously evaluated loads, material properties and other factors, the stress at these interaction points is determined.

To account for variations and uncertainties in models, different probabilistic approaches can be utilised to describe the distribution of mooring line stresses [47]. These stresses are usually non-Gaussian distributed and have a broad spectrum, but can also be represented by Weibull distributions. *Li et al.* [48] has developed

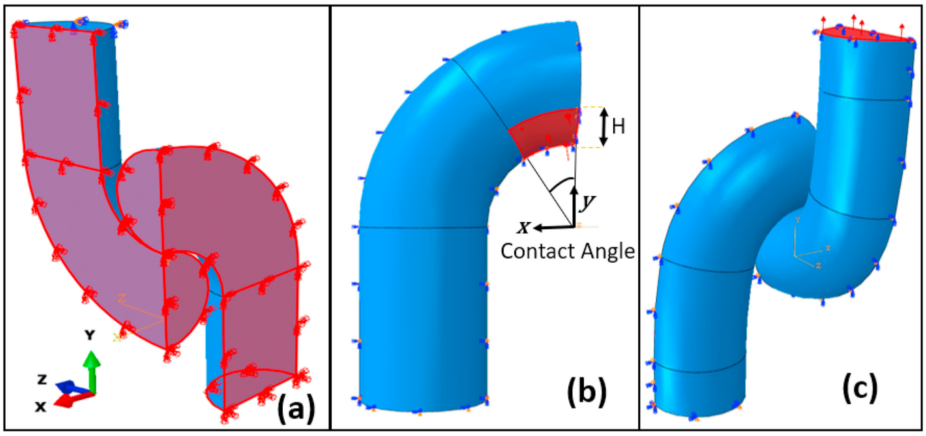

Figure 8: Modelling of important section of mooring chain segment interaction [15].

a gamma distribution and a modified gamma distribution to overcome the underestimation of fatigue damage by Weibull and Rayleigh distributions. This function handles non-Gaussianity very well and can be used for shallow water analysis and long term stress distributions, as they both have a high non-Gaussian portion. Further probabilistic methods can be used to implement uncertainties of loads in the fatigue analysis. These uncertainties can either be initiated from yearly variations or variations in the directions of waves, currents or winds. To describe stress uncertainties from short term sea state the Rayleigh distribution and for long-term statistics the Weibull distribution is a good fit [49, 50].

Models of mooring lines regarding tension often neglect out of plane bending.A modelling method to include bending using vector form intrinsic finite element methods was developed by *Zhang et al.* [7]. With this model a dynamic approach can be utilized, which is able to handle boundary conditions, as well as seabed interaction by implementing hydrodynamic drag, added mass and mooring line inertia [7].

After concluding the dynamic or quasi-static analyis and including possible improvements as mentioned above, the final result of the analysis are mooring line tensions or stresses, which can be converted into fatigue cycles using the rainflow counting method. The rainflow counting method can be used to determine the number of load cycles for a specific load from a time series and is based on the stress strain hysteresis loop. After the rainflow counting, the results can be used to determine the fatigue damage the mooring line will experience.

4.3.2 Prediction of the fatigue life using Palmgren Miner and stress, strain or tension curves

The most common procedure to determine fatigue lifetime assessment, as also described by *Du et al.* [20], is to use stress-, strain- or tension-cycle curves in combination with the Palmgren-Miner Hypothesis. A typical process for this can be seen in Figure 9. To determine how many of these cycles the mooring line

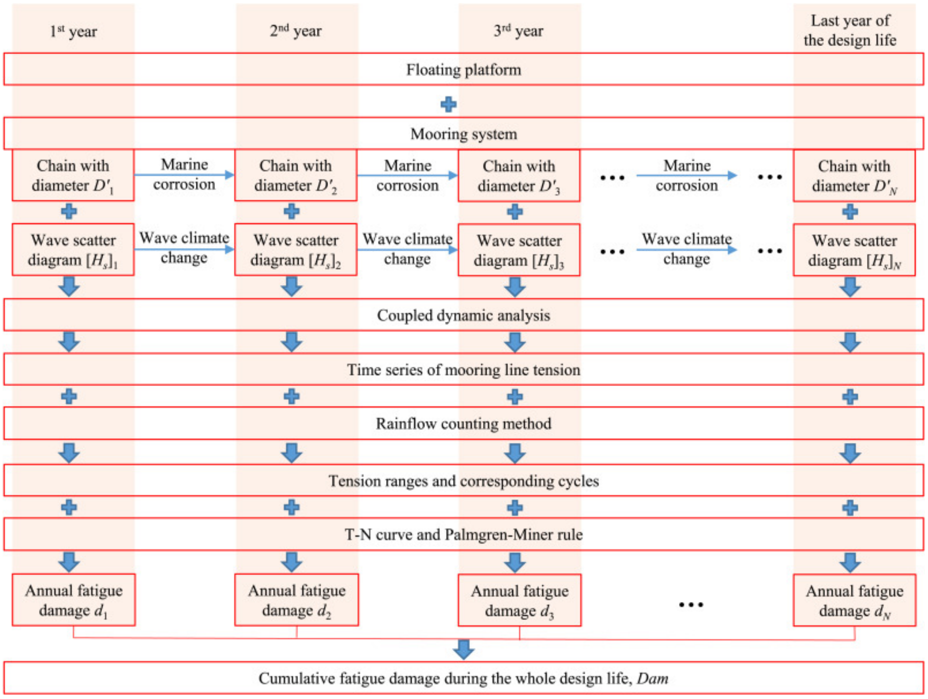

Figure 9: Example procedure of the fatigue damage estimation [20].

can withstand, the numerical results have to be compared to experimental results, which is often done by comparing the results to stress, strain or tension curves. These curves are based on experimental results, in which specimens of the to-be-tested material were exposed to cyclic loading.

To be able to compare the curves with the results, first linear accumulation of all sea states and their damage has to be executed. Therefore the Palmgren-Miner rule can be used, given in [20]. This is usually a summation for a specific sea state, but as given in [20] annual fatigue damage can be expressed through2.

$$D = \sum_i D_i = \sum_i \left(\frac{365 * 24 * P_i}{t} \sum_s \frac{n_{si}}{N_s}\right) \tag{2}$$

In this equation P_i represent the occurrence probability of the i-th seastate, t the simulation duration in hours, n_{si} and N_s being the number of tension cycles and the number to failure, respectively. In the stress curve, as presented in Figure 10 the stress loads are presented in regard to the load cycles.

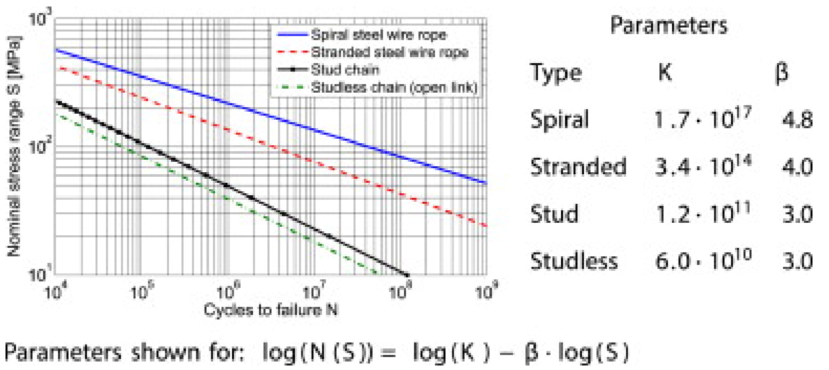

Figure 10: S-N curve, stress plotted against cycles until failure of a mooring line [51].

This stress curve can be described by the following equation:

$$N = KU^{-m} \tag{3}$$

Here U represent stress range, K the intercept parameter and m the slope of the curve.[38] Another option is to use the T-N curve, which considers the effective tension range with regard to loading cycles, where R_i equals U [35].

$$N_i = K_T R_i^{-M_T} \tag{4}$$

These two results can then be combined and used to estimate the lifetime of the mooring line

4.3.3 Neural networks for mooring line tension prediction

Based on these fatigue damage assessment approaches using Palmgren-Miner and FEM analysis, multiple researches have been executed to use neural networks to determine fatigue damage [52, 53, 54, 55]. Using neural network which can predict future tensions can be very helpful as they can be used in combination with sensors for mooring line failure detection. Here, the predicted mooring line tensions are used to create future movement patterns. If these do not overlap with the real movements, a mooring line failure can be detected quickly [56].

4.3.4 Prediction of lifetime using the crack growth equation

As the linear fatigue accumulation of Palmgren-Miner may lead to larger deviations compared to real fatigue damage accumulation, the crack growth method can also be used instead of S-N curves combined with Palmgren-Miner [40]. This method includes initial cracks, that can occur through welding, load testing or installation, considering the initial crack depth and the crack propagation [57]. The ultimate goal of this approach is to determine the final crack depth and fatigue life based on crack propagation due to stress. Example of the execution of this method is presented in Figure 11, which was used by *He at al.* [40].

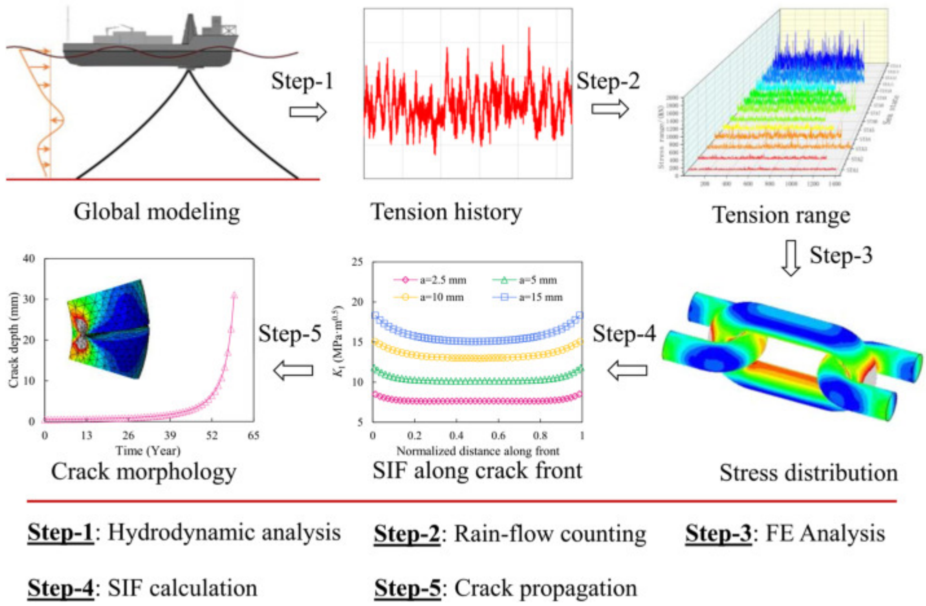

Figure 11: Example calculation of the fatigue damage assessment process using the crack growth equation[40].

In the process of the crack growth determination, tension ranges are determined as described in chapter 4.3.1. After using the rainflow counting method to determine the mooring tension the fatigue is determined through a fracture mechanics approach utilizing a fatigue crack growth predictive model. One of these models is the Paris law,represented in Equation 5 [58].

$$\frac{da}{dN} = C(\Delta K_{eq})^m, \Delta K_{eq} > \Delta K_{th} \tag{5}$$

In the Paris law, C and m represent Paris constants, K represents the amplitude of the stress intensity factor and K_{th} the fatigue threshold This is used when implementing the mooring line in ABAQUS. These cracks often occur at certain areas, as the bend section, the straight section and the crown, and thus are also modelled in these areas in ABAQUS, as sen in Figure 12.

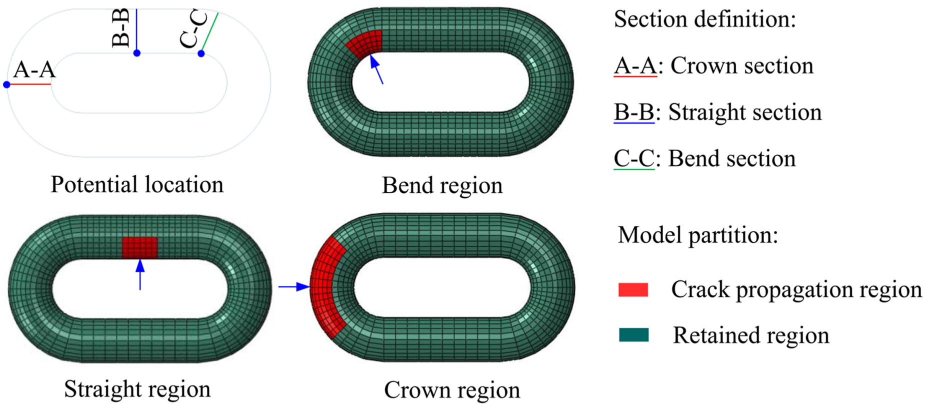

Figure 12: Fatigue crack prone regions of a mooring chain segment [40]

In the model given by *Mendoza et al.* [59]the most error-prone section was found to be the crown section with the crack probability of 86% . The initial cracks have two important details, the depth and the shape of the crack. The possible types of cracks and their modelling shapes in ABAQUS are given in table below.

Crack shape	**Modelling shape**	α
Convex	Almond shape	$\alpha > 0$
Concave	Sickle shape	$\alpha > 0$
Straight	Intermediate shape	$\alpha = 0$

Table 2: Modelling of crack types

If the crack depth cannot be determined by measurement, it can be selected as 0.5 mm as described by *Gao et al.* [38]. Another option, given by *Aursand et al.* [60], is the relative crack depth equation, presented in Equation 6.

$$\beta = \frac{\alpha}{D} \tag{6}$$

In the relative crack depth equation the crack depth is represented by α and the Diameter of the chain segment as D. C The critical crack depth is given as 12% of the chain diameter. All these factors are then used in the fracture mechanics approach to determine the actual crack depth and fatigue life. *Bergara et al.* [61] did a investigation for different finite element method modellings in ABAQUS, the FEM and the extended FEM(XFEM). In the extended version the crack propagation along a path can be simulated, through simulating stress around crack tip and the representation of stress corrosion factors. Stress intensity factors can be implemented in the model to identify stress around cracks, which helps in mooring integrity management.

$$\frac{da_d}{dN} = C_K(\Delta K_F^m) \tag{7}$$

with

$$K_F = Y\sigma\sqrt{\pi\alpha} \tag{8}$$

where K_f represent the stess intensity factor and Y is the stress intensity correction factor, based on geometry, and σ the stress acting on the mooring chain [38]. This is described by *Zhang et al.* [29] and determines the microcrack propagation in stress concentrated areas, the SCC, such as corrosion or the weld. In this process stress causes the protective layer of the mooring chain to be damaged and further initiation of microcracks. In these microcracks, corrosion can be initiated, leading to pitting corrosion, which causes microcracking. The quality of the weld has a major influence on the stress corrosion factor and must be chosen to suit the material, as well as the environmental and loading conditions. Also while using FEM modelling for crack growth evaluation not all the mooring line is modelled. *Gemilang et al.* [15] has proven that modelling only $1/8th$ of the mooring line is sufficient because it shows the most important interaction points. In this research also two kind of interactions, the pressure distribution and the contact interaction, between the chain segments were considered. In the analysis executed by *Thies et al.* [51] it was concluded that the fracture mechanics approach is a good tool to estimate fatigue life's of mooring lines. A disadvantage of the fracture mechanism approach can be that often the initial crack size is unknown.

4.4 Fatigue damage assessment including corrosion

Closer examination of mooring chains suggests that corrosion with wear and tear significantly shortens the life of the fatigue. As stated by *Lotfollahi et al.* [14], where non-corroded and corroded anchor line segments underwent load cycling tests, an anchor line loses a lot of mass due to corrosion and stress. This can be seen as a reduction in diameter, and as shown in Fig, this reduction in diameter leads to a reduction in the life of the anchor line. One method of modelling corrosion is to implement corrosion factors. Often, a corrosion factor is chosen for the entire mooring line, a diameter reduction per year that can be accumulated over the lifetime. As described by *Du et al.* [20] the diameter reduction is calculated as 0.4 mm/year, as 0.5 mm/year in combination with wear [43], or even up to 0.6 mm/year in [30]. Another implementation method is to determine the corrosion grades of mooring lines. Here, the condition of the mooring line is assessed on a scale of 1-7. One is the best condition without corrosion and seven is the most critical condition with pitting corrosion. To better incorporate corrosion in the fatigue assessment, combined with the mean load, *Lone et al.* [62] developed a new S-N curve that included corrosion and mean load on the mooring line. As noted by *Perez et al.* [63], the mean load has a decreasing effect on fatigue life, similar to the effect of corrosion. In the new S-N curve the mean load and corrosion are included as intercept parameters as well as in the Palmgren-Miner equation as seen in equation 10. The corrosion factor is given here as a grade indicator on a scale of one to seven.

$$A(\sigma_m, c) = 10^{b_0 + b_1 * g_1(\sigma_m) + b_2 * g_2(c)} \tag{9}$$

Where A is the intercept parameter , b0-b2 are coefficients and further $g_1(\sigma_m)$ being the function of the mean stress and $g_2(c)$ the function of corrosion. The final curve is based on an adaptation of the original S-N equation 13 seen below in combination with the Palmgren-Miner adapted equation given in 10

$$D = \sum_i \frac{n_i * s_i^m}{A(\sigma_{m,i}, c_i}) \tag{10}$$

Disadvantages of this curve are that the curve is dependent on a minimum breaking point at which it was tested, which is 20% and that the selection of corrosion grades are fairly subjective. Based on the new S-N curve, a probabilistic fatigue model was developed to include load uncertainties and other effects impacting the fatigue capacity of a mooring line [64]. Here a probabilistic model for the corrosion history of the model was implemented, using an updated Palmgren-Miner Theorem to calculate the annual fatigue damage, as seen in 11.

$$D = \sum_{k=1}^{N_p} \frac{Z_k^*}{10^{b_0 + b_2 * g_{2,k}^*}} + \sum_{k=N_p+1}^{N_p+N_f} \frac{Z_k^*}{10^{b_0 + b_2 * g_{2,k}^*}} \tag{11}$$

where the first part is the prior damage and the second the future damage. N_p and N_f are the amounts of prior and future years. Z_k being the fatigue load for the k-th year, and b0 and b2 accounting for uncertainties of the capacity model . The corrosion grade was improved with a uncertainty factor and is given as $g_{2,k}$ Combining these two researches, *Lone et al.* [65] a more extensive research. A global sensitivity analysis was executed on the basis of the improved formulations for corrosion grades and fatigue damage, as given in equations **??** and 10. On the basis of this and a graph was developed, which is presented in figure13 and shows different estimations for the probability of failure based on corrosion and mean load variations. As mentioned by

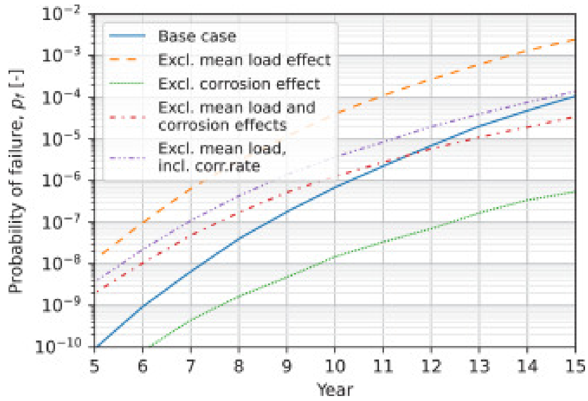

Figure 13: Probability of failure plotted against immersion years of the mooring line with different cases regarding mean load and corrosion [65].

Qvale et al. [33], corrosion can have positive and negative effects on the fatigue crack growth. Although the first impression is that that corrosion only increase material degradation, it can also be reduced by it. Through either the development of corrosion products in the crack, and following the crack closure initiation, or the blunting of crack tips which reduces stresses can decrease the development of fatigue cracks.

4.5 Weak points along mooring lines

To determine points along the mooring line which have a higher failure probability, multiple factors besides stress and corrosion have to be considered. For one, the choice between catenary or taut mooring can influence fatigue damage. As noted in [66], catenary systems have a longer fatigue life than taut mooring lines. This can be explained by the pre-tension in the mooring line. In general, the pretension has a significant effect on the fatigue life of the mooring line, and reducing the pretension in the mooring line can significantly increase the fatigue life of a mooring line. Even though the lifetime of a catenary system is longer, it experiences higher loads during it [67]. Unlike a taut system which can compensate loads through elongation of the mooring line, catenary mooring lines are often lifted off the seabed. Water depth also has an effect on fatigue life. A mooring system in shallow water will have a shorter fatigue life than one in deep water. This was taken into account by [68], who found that the excitation loads increase as the water depth decreases. In particular, with respect to the taut mooring system, it was shown that there are stronger dynamic effects on the mooring line, caused by the higher excitation, and thus a reduced fatigue life in shallow water [66, 68]. Another effect on the mooring line is the interaction between the chain and the seabed. This has been shown to reduce the service life of mooring lines, particularly for low frequency motions. Another important aspect to consider is the material of the mooring line. More and more mooring lines are combined with chain segments at the top and bottom and a polyester core in the permanent immersion zone. The fatigue life is influenced by the higher durability of polyester, but higher fatigue increase at the connection points. The main areas of concern are the fairlead, the end of the top chain, the top of the bottom chain and the point where the chain interacts with the seabed, as shown in Figure 14.

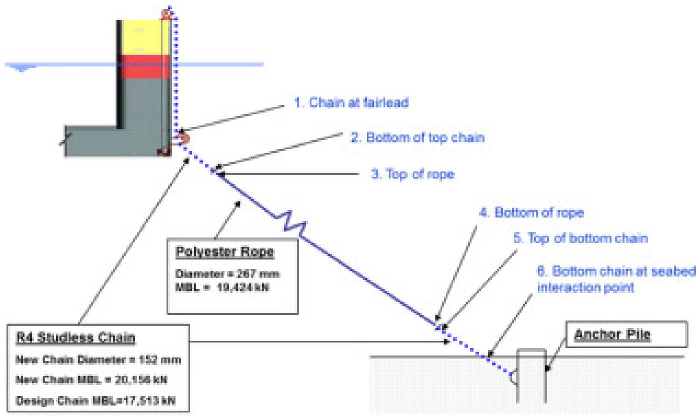

Figure 14: Example of a mooring line assembly, indicating possible weak points along the line [66].

Wu et al. [66] concludes that for tensioned mooring systems, the most critical point for the occurrence of fatigue damage is the top of the bottom chain. This may also be the most critical point for the catenary mooring line, but the chain-seabed interaction point also shows a high likelihood of fatigue damage. The dominant case here is determined by the decision of the friction factor and the length of the mooring chain placed on the seabed. Research by *Barrera et al.* [69] has showed that tension increases for example if the mooring line is interacting with sand sea floor instead of a seafloor covered with rocks by up to 15 %. Another interesting aspect to take into account is that the proof load, which is used for testing of the mooring lines can cause permanent elongation and residual stresses [70]. As described by *Yuan et al.* [71] to decrease mooring line tensions in some parts of the chain, clamped weights and buoys can be implemented in the setup. These two points of connection to the mooring chain could be increasing the wear. However, unfortunately this has not yet been investigated in research.

5 Reflection

As presented in chapter 4, a great deal of research has been carried out to investigate the degradation of mooring lines. Comparing the results of the literature review with the preliminary research questions, it can be seen that some answers have been found, but there are also gaps that have not been investigated in relation to the fatigue life assessment of mooring lines.

How do corrosion and fatigue affect the estimated service life of a mooring line?

Corrosion and fatigue have been shown to reduce the fatigue life of mooring lines. As discussed in chapter 4.2, pitting corrosion is initiated after the installation of the mooring line and leads to uniform corrosion in the later stages, resulting in a reduction in the diameter of the mooring chain segments. Fatigue, as discussed in Section 4.3, will result in fatigue cracks in the bend, straight and crown areas of the chain element.

How are fatigue and corrosion considered in the design of mooring lines?

One aspect that becomes very noticeable when comparing mooring line corrosion research is that in many numerical fatigue life evaluations, corrosion has either been neglected or included in a very conservative manner as a constant factor. A comparison of the constant value for the total mooring line length with the experimental data for different depths given in Chapter 4.2 shows that in some cases the corrosion is too conservative or not sufficient. Although [28] has shown that the entire surface of a mooring line is altered, which supports the idea of implementing corrosion as a reduction in diameter, the constant corrosion factor can be quite inaccurate with respect to immersion time and depth. In other research, corrosion grades have been used to determine the chain degradation process and, thus how far a chain has corroded. This type of implementation can be problematic as the same investigator must decide the corrosion grades. If more than one person investigating the same chain, the decision on the corrosion grade can vary. For this reason, an equation has been introduced in chapter 4.4 to take account of uncertainties .

Fatigue is implemented using S-N curves or calculated using the crack growth equation. S-N curves are based on the stress-cycles a mooring chain can endure during it's lifetime. The crack propagation method, as presented in chapter 4.3.4 estimates the development of cracks due to residual stresses in the surface. The critical crack depth can be used to determine the service life of a mooring chain by determining the crack evolution. In addition, the effects of corrosion and fatigue on the chain have also been considered in a number of studies.

How do corrosion and fatigue affect each other?

Authors of [65] have extensively researched the effects of corrosion and mean load on fatigue and developed a new S-N curve considering both. This research was carried out on FPSOs, where risers were also included in the movements of the floater [64] and therefore might not be entirely applicable for FOWT. Another approach presented to investigate fatigue and corrosion life reduction is fracture mechanics approaches, as the SCC. This phenomenon occurs when fatigue and corrosion are combined, as described in the chapter 4.3.4. Though the cyclic stress, stress concentrations occur in the mooring chain segments, leading to micro cracks of the surface and to a damage of the protective film. Through the damage water can reach the microcracks and corrosion is initiated on the mooring chain. As described by *Zhang et al.* [29] the occurrence of pitting corrosion influences the SCC by promoting the formation of microcracks due to corrosion at the pits. This can be explained through the higher stress concentration on corrosion pits, leading to the initiation of cracks. The disadvantage of this approach is that the influence of corrosion on the cracks is sometimes not very clear. As shown by [33], corrosion can also lead to closure of the initial cracks or blunting of the crack tip, depending on the loading. Further through the reduction in diameter due to corrosion, the critical crack depth being reached more rapidly, as it is dependent on the diameter of the anchor chain.

Are there areas of increased deterioration along the mooring line?

As discussed in section 4.5, there are locations along the mooring line that are prone to failure. Unfortunately, there has not been much research into these locations, particularly with regard to corrosion and fatigue. Based on these findings, the preliminary research questions formed a good basis for research, from which the main Research Question (RQ) was found for the following Master's thesis, which will be carried out under the following focus:

RQ (1): How can fatigue and corrosion be modelled to identify weak points along the mooring lines of floating offshore wind turbines?

The following sub RQs will be addressed in more detail:

1. How can fatigue be accurately modelled along the mooring line?
2. How can corrosion along the mooring line be accurately modelled?
3. How do fatigue and corrosion interact?
4. How can the weak points be improved?

A proposed methodology is presented in Section 6 to answer the main RQ and the above-mentioned sub RQs questions.

6 Proposed methodology for the subsequent master thesis

Based on the previous literature research and the new research questions, a methodology for the following master thesis was determined. A schematic of the methodology can be seen in Figure 15. In phase one of the

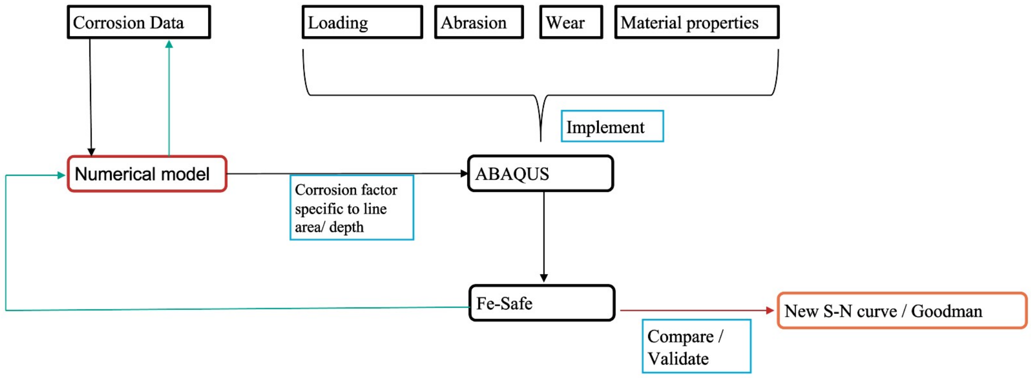

Figure 15: Schematic of methodology

thesis the input data for the model will be determined. Corrosion data and equations from previous research will be used to determine corrosion development over the length of the mooring line. Other inputs to the finite element model will be loads, abrasion, wear and the specific material properties of the mooring line. Loads will be determined either by time domain dynamic analysis in combination with the Morrison equation and Jonswap, or based on experimental data deemed reliable. Wear will be applied at specific points where the mooring lines interact with buoys, clamp weights, the seabed, connectors or the FOWT itself. Abrasion and friction on the seabed will be determined by research results.

In phase two, a chain segment model is implemented in ABAQUS to achieve the objectives of modelling corrosion and fatigue along the mooring line and to identify possible weak points. This model of approximately two or three chain segments will be tested for different locations of the mooring lines with different inputs. ABAQUS can then be used to simulate the stress distribution on the individual mooring line chain segments, as well as the stress cycles.

In phase three the outcome of the ABAQUS model is used to numerically derive a stress history and determine a stress range using the rainflow counting method to determine an S-N curve. To verify the research approach, the results are then compared and confirmed with the new curves by *Lone et al.* [65]. As an important focus is on the weak points of the mooring line, different simulations will be used to find weak points for different parts of the mooring line. Improvements will then be proposed for those areas. For the development of this project within the framework of a Master's thesis, a specific time frame is given, therefore a possible structure for this project in terms of time management has been developed in the following GANTT chart.

GANTT Chartt

Period Highlight: 1

Plan Duration | Actual Start | % Complete | Actual (beyond plan) | % Complete (beyond plan)

TASK	PLAN START	PLAN DURATION	ACTUAL START	ACTUAL DURATION	PERCENT COMPLETE
Master thesis	**06.03.2023**	**24 Weeks**			
Literature research	1	4	0	0	0%
Development of corrosion model	1	4	0	0	0%
Determination of input for FEM model	3	5	0	0	0%
Development of FEM model	5	6	0	0	0%
Simulation	9	4	0	0	0%
Comparison to current research	12	3	0	0	0%
Improvement of model	14	1	0	0	0%
Simulation using improved model	15	2	0	0	0%
Validation	15	3	0	0	0%
Thesis formulation	12	10	0	0	0%
Masterthesis hand-in	22	1	0	0	0%
Masterthesis correction	23	2	0	0	0%
Documentation	1	20	0	0	0%

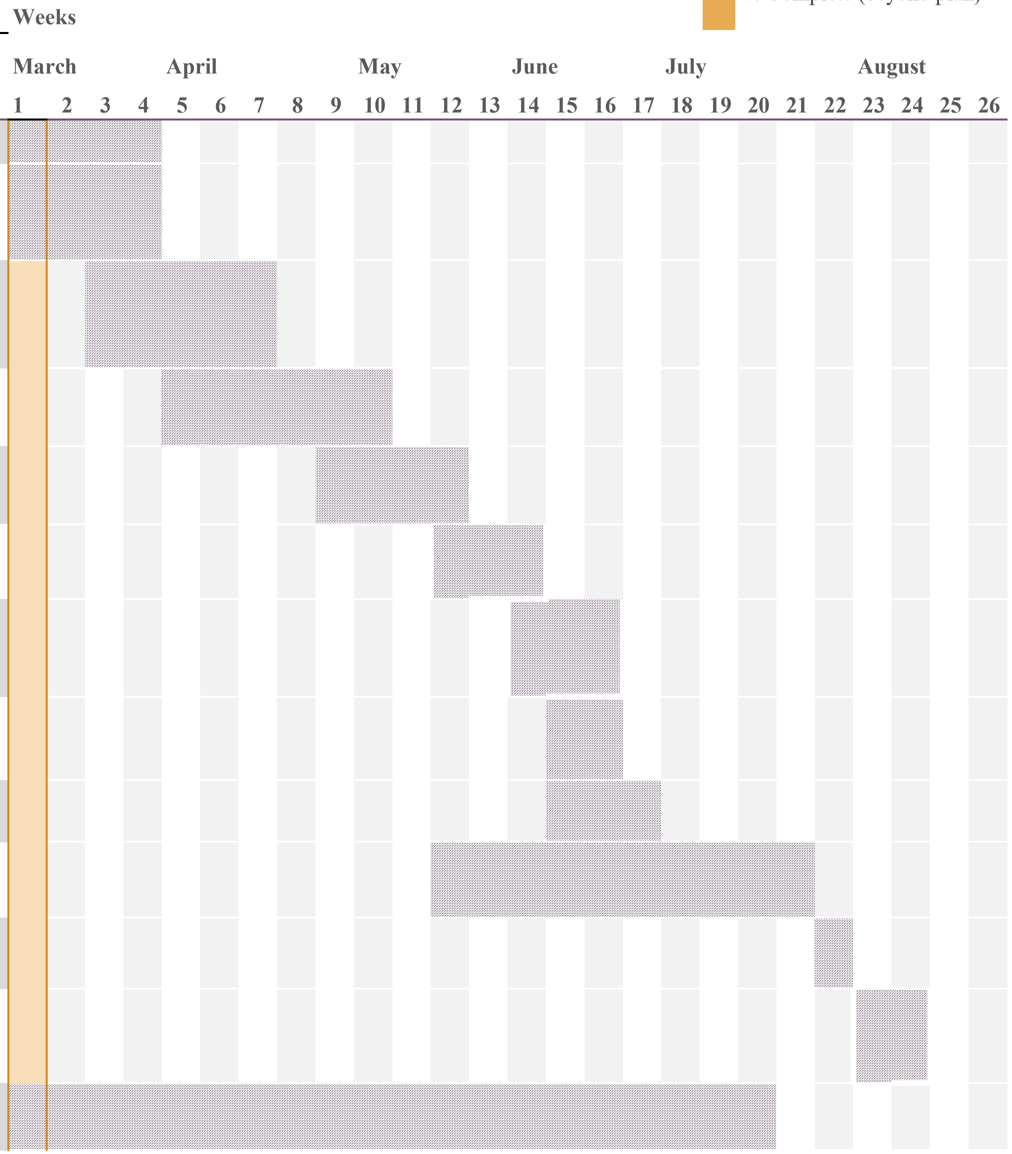

References

[1] Rebecca Williams, Feng Zhao, and Joyce Lee. Global Offshore Wind Report 2022. Technical report, Global Wind Energy Council, Brussels, 6 2022.

[2] Josep Lloret, Antonio Turiel, Jordi Solé, Elisa Berdalet, Ana Sabatés, Alberto Olivares, Josep Maria Gili, Josep Vila-Subirós, and Rafael Sardá. Unravelling the ecological impacts of large-scale offshore wind farms in the Mediterranean Sea. *Science of the Total Environment*, 824, 6 2022.

[3] Charalampos Baniotopoulos. Advances in Floating Wind Energy Converters. *Energies 2022, Vol. 15, Page 5658*, 15(15):5658, 8 2022.

[4] E. Fontaine, A. Kilner, C. Carra, D. Washington, K. T. Ma, A. Phadke, D. Laskowski, and G. Kusinski. Industry Survey of Past Failures, Pre-emptive Replacements and Reported Degradations for Mooring Systems of Floating Production Units. *Proceedings of the Annual Offshore Technology Conference*, 3:2038–2051, 5 2014.

[5] Kai Tung Ma, Yong Luo, Thomas Kwan, and Yongyan Wu. Mooring system engineering for offshore structures. *Mooring System Engineering for Offshore Structures*, pages 1–350, 1 2019.

[6] Mehmet Bilgili, Abdulkadir Yasar, and Erdogan Simsek. Offshore wind power development in Europe and its comparison with onshore counterpart. *Renewable and Sustainable Energy Reviews*, 15(2):905–915, 2011.

[7] Yu Zhang, Wei Shi, Dongsheng Li, Xin Li, and Yuanfeng Duan. Development of a numerical mooring line model for a floating wind turbine based on the vector form intrinsic finite element method. *Ocean Engineering*, 253, 6 2022.

[8] Vanja Westerberg, Jette Bredahl Jacobsen, and Robert Lifran. Offshore wind farms in Southern Europe – Determining tourist preference and social acceptance. *Energy Research & Social Science*, 10:165–179, 11 2015.

[9] Yang Yang, Musa Bashir, Chun Li, and Jin Wang. Investigation on mooring breakage effects of a 5MW barge-type floating offshore wind turbine using F2A. *Ocean Engineering*, 233, 8 2021.

[10] Yusuf Alper Kaplan. Overview of wind energy in the world and assessment of current wind energy policies in Turkey. *Renewable and Sustainable Energy Reviews*, 43:562–568, 3 2015.

[11] Lena Bergström, Lena Kautsky, Torleif Malm, Rutger Rosenberg, Magnus Wahlberg, Nastassja Åstrand Capetillo, and Dan Wilhelmsson. Effects of offshore wind farms on marine wildlife—a generalized impact assessment. *Environmental Research Letters*, 9(3):034012, 3 2014.

[12] Kaoshan Dai, Anthony Bergot, Chao Liang, Wei Ning Xiang, and Zhenhua Huang. Environmental issues associated with wind energy – A review. *Renewable Energy*, 75:911–921, 3 2015.

[13] He Li, H. Díaz, and C. Guedes Soares. A failure analysis of floating offshore wind turbines using AHP-FMEA methodology. *Ocean Engineering*, 234:109261, 8 2021.

[14] Amin Lotfollahi Yaghin and Robert E. Melchers. Long-term inter-link wear of model mooring chains. *Marine Structures*, 44:61–84, 12 2015.

[15] G. M. Gemilang, P. A.S. Reed, and A. J. Sobey. Selection of appropriate numerical models for modelling the stresses in mooring chains. *Marine Structures*, 75:102864, 1 2021.

[16] Chenglin Zhang, Shiming Wang, Shuangyi Xie, Jiao He, Jian Gao, and Changfeng Tian. Effects of mooring line failure on the dynamic responses of a semisubmersible floating offshore wind turbine including gearbox dynamics analysis. *Ocean Engineering*, 245, 2 2022.

[17] Y. H. Bae, M. H. Kim, and H. C. Kim. Performance changes of a floating offshore wind turbine with broken mooring line. *Renewable Energy*, 101:364–375, 2 2017.

[18] Minwoong Chung, Seungjun Kim, Kanghyeok Lee, and Do Hyoung Shin. Detection of damaged mooring line based on deep neural networks. *Ocean Engineering*, 209:107522, 8 2020.

[19] Omar El Beshbichi, Yihan Xing, and Muk Chen Ong. Comparative dynamic analysis of two-rotor wind turbine on spar-type, semi-submersible, and tension-leg floating platforms. *Ocean Engineering*, 266:112926, 12 2022.

[20] Junfeng Du, Hongchao Wang, Shuqing Wang, Xiancang Song, Junrong Wang, and Anteng Chang. Fatigue damage assessment of mooring lines under the effect of wave climate change and marine corrosion. *Ocean Engineering*, 206:107303, 6 2020.

[21] Robert B. Gordon, Martin G. Brown, and Eric M. Allen. Mooring Integrity Management: A State-of-the-Art Review. *Proceedings of the Annual Offshore Technology Conference*, 1:577–595, 5 2014.

[22] R. Nevshupa, I. Martinez, S. Ramos, and A. Arredondo. The effect of environmental variables on early corrosion of high–strength low–alloy mooring steel immersed in seawater. *Marine Structures*, 60:226–240, 7 2018.

[23] Robert E. Melchers, Torgeir Moan, and Zhen Gao. Corrosion of working chains continuously immersed in seawater. *Journal of Marine Science and Technology*, 12(2):102–110, 6 2007.

[24] Juliusz Orlikowski, Michał Szociński, Krzysztof Żakowski, Piotr Igliński, Kinga Domańska, and Kazimierz Darowicki. Actual field corrosion rate of offshore structures in the Baltic Sea along depth profile from water surface to sea bed. *Ocean Engineering*, 265:112545, 12 2022.

[25] Wenkui Hao, Zhiyong Liu, Wei Wu, Xiaogang Li, Cuiwei Du, and Dawei Zhang. Electrochemical characterization and stress corrosion cracking of E690 high strength steel in wet-dry cyclic marine environments. *Materials Science and Engineering A*, 710:318–328, 1 2018.

[26] Øystein Gabrielsen, Turid Liengen, and Solfrid Molid. Microbiologically Influenced Corrosion on seabed chain in the North Sea. *Proceedings of the International Conference on Offshore Mechanics and Arctic Engineering - OMAE*, 3, 2018.

[27] Xuewei Zhang, Suli Zhao, Zheng Wang, Jinxu Li, and Lijie Qiao. The pitting to uniform corrosion evolution process promoted by large inclusions in mooring chain steels. *Materials Characterization*, 181:111456, 11 2021.

[28] Y. Argouarc'h and R. Creac'hcadec. Registration method for the analysis of mooring chain links degraded by corrosion and wear. *Ocean Engineering*, 250:110877, 4 2022.

[29] Xuewei Zhang, Weijie Wu, Hao Fu, and Jinxu Li. The effect of corrosion evolution on the stress corrosion cracking behavior of mooring chain steel. *Corrosion Science*, 203:110316, 7 2022.

[30] Ángela Angulo, Graham Edwards, Slim Soua, and Tat-Hean Gan. Mooring Integrity Management: Novel Approaches Towards In Situ Monitoring. *Structural Health Monitoring - Measurement Methods and Practical Applications*, 6 2017.

[31] Julien Lardier, Torgeir Moan, and Zhen Gao. Fatigue Reliability of Catenary Mooring Lines Under Corrosion Effect. *Proceedings of the International Conference on Offshore Mechanics and Arctic Engineering - OMAE*, 2:351–358, 7 2009.

[32] Mst Kamrunnahar and Mirna Urquidi-Macdonald. Prediction of corrosion behavior using neural network as a data mining tool. *Corrosion Science*, 52(3):669–677, 3 2010.

[33] Paul Qvale, Håkon O. Nordhagen, Sigmund K. Ås, and Bjørn H. Skallerud. Effect of long periods of corrosion on the fatigue lifetime of offshore mooring chain steel. *Marine Structures*, 85:103236, 9 2022.

[34] Hui Min Hou, Guo Hai Dong, Tiao Jian Xu, Yun Peng Zhao, Chun Wei Bi, and Fu Kun Gui. Fatigue reliability analysis of mooring system for fish cage. *Applied Ocean Research*, 71:77–89, 2 2018.

[35] Carlos Barrera, Tommaso Battistella, Raúl Guanche, and Iñigo J. Losada. Mooring system fatigue analysis of a floating offshore wind turbine. *Ocean Engineering*, 195, 1 2020.

[36] Thomas Sauder, Philippe Mainçon, Erling Lone, and Bernt J. Leira. Estimation of top tensions in mooring lines by sensor fusion. *Marine Structures*, 86:103309, 11 2022.

[37] Carlos Barrera, Iñigo J. Losada, Raúl Guanche, and Lars Johanning. The influence of wave parameter definition over floating wind platform mooring systems under severe sea states. *Ocean Engineering*, 172:105–126, 1 2019.

[38] Xifeng Gao, Xiaoyong Liu, Xutian Xue, and Nian Zhong Chen. Fracture mechanics-based mooring system fatigue analysis for a spar-based floating offshore wind turbine. *Ocean Engineering*, 223, 3 2021.

[39] A. Campanile, V. Piscopo, and A. Scamardella. Mooring design and selection for floating offshore wind turbines on intermediate and deep water depths. *Ocean Engineering*, 148:349–360, 1 2018.

[40] Wentao He, Shihui Cao, Zhiqiang Hu, De Xie, Zhengyi Zhang, and Changzi Wang. Numerical evaluation on fatigue crack growth and life predictions of an FPSO mooring system. *Ocean Engineering*, 265:112501, 12 2022.

[41] Sheng Xu and C. Guedes Soares. Evaluation of spectral methods for long term fatigue damage analysis of synthetic fibre mooring ropes based on experimental data. *Ocean Engineering*, 226, 4 2021.

[42] Matthew Hall, Brad Buckham, and Curran Crawford. Evaluating the importance of mooring line model fidelity in floating offshore wind turbine simulations. *Wind Energy*, 17(12):1835–1853, 12 2014.

[43] Xutian Xue, Nian Zhong Chen, Yongyan Wu, Yeping Xiong, and Yunhua Guo. Mooring system fatigue analysis for a semi-submersible. *Ocean Engineering*, 156:550–563, 5 2018.

[44] Hedi Basbas, Yong Chao Liu, Salah Laghrouche, Mickaël Hilairet, and Franck Plestan. Review on Floating Offshore Wind Turbine Models for Nonlinear Control Design. *Energies 2022, Vol. 15, Page 5477*, 15(15):5477, 7 2022.

[45] Murray Rudman and Paul W. Cleary. The influence of mooring system in rogue wave impact on an offshore platform. *Ocean Engineering*, 115:168–181, 3 2016.

[46] Matthew Hall and Andrew Goupee. Validation of a lumped-mass mooring line model with DeepCwind semisubmersible model test data. *Ocean Engineering*, 104:590–603, 6 2015.

[47] Huajun Li, Junfeng Du, Shuqing Wang, Mingyuan Sun, and Anteng Chang. Investigation on the probabilistic distribution of mooring line tension for fatigue damage assessment. *Ocean Engineering*, 124:204–214, 9 2016.

[48] Junfeng Du, Anteng Chang, Shuqing Wang, Mingyuan Sun, Junrong Wang, and Huajun Li. Multi-mode reliability analysis of mooring system of deep-water floating structures. *Ocean Engineering*, 192:106517, 11 2019.

[49] C. Rendón-Conde and E. Heredia-Zavoni. Reliability assessment of mooring lines for floating structures considering statistical parameter uncertainties. *Applied Ocean Research*, 52:295–308, 8 2015.

[50] R. Montes-Iturrizaga, E. Heredia-Zavoni, F. Silva-González, and D. Straub. Nested reliability analysis of mooring lines for floating systems. *Applied Ocean Research*, 34:107–115, 1 2012.

[51] Philipp R. Thies, Lars Johanning, Violette Harnois, Helen C.M. Smith, and David N. Parish. Mooring line fatigue damage evaluation for floating marine energy converters: Field measurements and prediction. *Renewable Energy*, 63:133–144, 3 2014.

[52] Yixuan Mao, Tianqi Wang, and Menglan Duan. A DNN-based approach to predict dynamic mooring tensions for semi-submersible platform under a mooring line failure condition. *Ocean Engineering*, 266:112767, 12 2022.

[53] Chun Bao Li, Joonmo Choung, and Myung Hyun Noh. Wide-banded fatigue damage evaluation of Catenary mooring lines using various Artificial Neural Networks models. *Marine Structures*, 60:186–200, 7 2018.

[54] Chun Bao Li and Joonmo Choung. Fatigue damage analysis for a floating offshore wind turbine mooring line using the artificial neural network approach. *Ships and Offshore Structures*, 12:S288–S295, 3 2017.

[55] Yuliang Zhao, Sheng Dong, Fengyuan Jiang, and Atilla Incecik. Mooring tension prediction based on BP neural network for semi-submersible platform. *Ocean Engineering*, 223:108714, 3 2021.

[56] Amir Muhammed Saad, Florian Schopp, Rodrigo A. Barreira, Ismael H.F. Santos, Eduardo A. Tannuri, Edson S. Gomi, and Anna H.Reali Costa. Using Neural Network Approaches to Detect Mooring Line Failure. *IEEE Access*, 9:27678–27695, 2021.

[57] Pedro M.Calas Lopes Pacheco, Marcelo Amorim Savi, Paulo Pedro Kenedi, Jorge Carlos Ferreira Jorge, and Hugo Gama Dos Santos. Finite element residual stress analysis applied to offshore studless chain links. *Proceedings of the International Conference on Offshore Mechanics and Arctic Engineering - OMAE*, 2:935–944, 2004.

[58] N. Pugno, M. Ciavarella, P. Cornetti, and A. Carpinteri. A generalized Paris' law for fatigue crack growth. *Journal of the Mechanics and Physics of Solids*, 54(7):1333–1349, 7 2006.

[59] Jorge Mendoza, Per J. Haagensen, and Jochen Köhler. Analysis of fatigue test data of retrieved mooring chain links subject to pitting corrosion. *Marine Structures*, 81:103119, 1 2022.

[60] Mads Aursand and Bjørn H. Skallerud. Mode I stress intensity factors for semi-elliptical fatigue cracks in curved round bars. *Theoretical and Applied Fracture Mechanics*, 112:102904, 4 2021.

[61] A. Bergara, A. Arredondo, J. Altuzarra, and J. M. Martínez-Esnaola. Fatigue crack propagation analysis in offshore mooring chains and the influence of manufacturing residual stresses. *Ocean Engineering*, 257:111605, 8 2022.

[62] Erling N Lone, Thomas Sauder, Kjell Larsen, Equinor Asa, and Bernt J Leira. FATIGUE ASSESSMENT OF MOORING CHAIN CONSIDERING THE EFFECTS OF MEAN LOAD AND CORROSION. 2021.

[63] Imanol Martinez Perez, Philippe Bastid, Andrei Constantinescu, and Vengatesan Venugopal. Multiaxial fatigue analysis of mooring chain links under tension loading: Influence of mean load and simplified assessment. *Proceedings of the International Conference on Offshore Mechanics and Arctic Engineering - OMAE*, 3, 2018.

[64] Erling N. Lone, Thomas Sauder, Kjell Larsen, and Bernt J. Leira. Probabilistic fatigue model for design and life extension of mooring chains, including mean load and corrosion effects. *Ocean Engineering*, 245, 2 2022.

[65] Erling N. Lone, Thomas Sauder, Kjell Larsen, and Bernt J. Leira. Fatigue reliability of mooring chains, including mean load and corrosion effects. *Ocean Engineering*, 266:112621, 12 2022.

[66] Yongyan Wu, Tao Wang, Øyvind Eide, and Kevin Haverty. Governing factors and locations of fatigue damage on mooring lines of floating structures. *Ocean Engineering*, 96:109–124, 3 2015.

[67] Magnus Thorsen Bach-Gansmo, Stian Kielland Garvik, Jonas Bjerg Thomsen, and Morten Thøtt Andersen. Parametric Study of a Taut Compliant Mooring System for a FOWT Compared to a Catenary Mooring. *Journal of Marine Science and Engineering 2020, Vol. 8, Page 431*, 8(6):431, 6 2020.

[68] Wei Shi, Lixian Zhang, Madjid Karimirad, Constantine Michailides, Zhiyu Jiang, and Xin Li. Combined effects of aerodynamic and second-order hydrodynamic loads for floating wind turbines at different water depths. *Applied Ocean Research*, 130, 1 2023.

[69] Carlos Barrera, Raúl Guanche, and Iñigo J. Losada. Experimental modelling of mooring systems for floating marine energy concepts. *Marine Structures*, 63:153–180, 1 2019.

[70] Ankit Sachan and Yoo Sang Choo. Mooring chain strength tests and ductile failure modeling using micromechanics and phenomenology based failure models. *Ocean Engineering*, 195, 1 2020.

[71] Zhi Ming Yuan, Atilla Incecik, and Chunyan Ji. Numerical study on a hybrid mooring system with clump weights and buoys. *Ocean Engineering*, 88:1–11, 9 2014.

B Appendix B

Label	Section	DEL in x-direction [KN]	DEL in z-direction [KN]	Hydrostatic pressure [Mpa]	Nominal stress range	Lifecycles	Corrosion rate first year [mm/year]	Nominal stress range [MPa]	Lifecycles [E6]
Load 1	Top node	64.619	62.97	-0.20	39.33	226.15	0.12	95.31	6.50
	Middle node	75.961	49.84	-1.16	43.24	154.85	0.11	104.58	4.48
	Bottom node	94.055	13.61	-1.97	57.32	50.12	0.11	117.09	2.85
Load 2	Top node	64.723	62.84	-0.20	39.37	225.32	0.120	95.40	6.48
	Middle node	75.954	49.84	-1.16	43.24	154.85	0.114	104.58	4.48
	Bottom node	94.043	13.61	-1.97	57.32	50.12	0.105	117.09	2.85
Load 3	Top node	65.16	63.39	-0.20	39.50	222.26	0.12	96.21	6.26
	Middle node	75.954	49.84	-1.16	43.24	154.85	0.114	104.58	4.49
	Bottom node	94.04	13.61	-1.97	57.32	50.12	0.105	117.09	2.85
Load 4	Top node	65.17	63.39	-0.20	39.50	222.26	0.12	96.21	6.27
	Middle node	76.347	50.10	-1.16	43.35	153.19	0.11	104.85	4.44
	Bottom node	94.9	13.73	-1.97	57.65	48.98	0.10	117.72	2.79
Load5	Top node	65.15	63.38	-0.20	39.50	222.26	0.12	96.21	6.27
	Middle node	76.342	50.1	-1.16	43.35	153.19	0.11	104.85	4.44
	Bottom node	94.78	13.72	-1.97	57.61	49.13	0.10	117.63	2.80
Load 6	Top node	79.378	72.93	-0.1946	44.15	142.37	0.12	106.65	4.15
	Middle node	92.678	58.46	-1.13	56.24	54.09	0.11	116.82	2.88
	Bottom node	111.41	19.06	-1.95	64.00	32.26	0.10	104.04	4.58
Load 7	Top node	79.91	73.41	-0.19	43.17	155.76	0.12	106.38	4.19
	Middle node	93.712	59.11	-1.12	56.24	54.09	0.11	117.63	2.8
	Bottom node	112.22	19.45	-1.95	64.31	31.63	0.10	130.41	1.86
Load 8	Top node	79.911	73.42	-0.19	44.32	140.30	0.12	106.38	4.19
	Middle node	93.702	59.10	-1.13	56.64	52.59	0.11	117.63	2.80
	Bottom node	112.46	17.99	-1.94	64.15	31.95	0.106	130.41	1.86

Table 22: Load cases with a high probability of occurrence examined for corrosion influence.